



## New Roles for the Gamma Rhythm: Population Tuning and Preprocessing for the Beta Rhythm

METTE S. OLUFSEN

*Department of Mathematics, North Carolina State University, Raleigh, NC 27659-8205*

MILES A. WHITTINGTON

*School of Biomedical Sciences, The University of Leeds, Leeds LS2 9NL, UK*

MARCELO CAMPERI

*Physics Department, University of San Francisco, San Francisco, CA 94117*

NANCY KOPELL

*Center for BioDynamics and Department of Mathematics, Boston University, Boston, MA 02215*

*nk@bu.edu*

*Received January 22, 2002; Revised June 28, 2002; Accepted July 16, 2002*

Action Editor: Carson C. Chow

**Abstract.** Gamma (30–80 Hz) and beta (12–30 Hz) oscillations such as those displayed by *in vitro* hippocampal (CA1) slice preparations and by *in vivo* neocortical EEGs often occur successively, with a spontaneous transition between them. In the gamma rhythm, pyramidal cells fire together with the interneurons, while in the beta rhythm, pyramidal cells fire on a subset of cycles of the interneurons. It is shown that gamma and beta rhythms have different properties with respect to creation of cell assemblies. In the presence of heterogeneous inputs to the pyramidal cells, the gamma rhythm creates an assembly of firing pyramidal cells from cells whose drive exceeds a threshold. During the gamma to beta transition, a slow outward potassium current is activated, and as a result the cell assembly vanishes. The slow currents make each of the pyramidal cells fire with a beta rhythm, but the field potential of the network still displays a gamma rhythm. Hebbian changes of connections among the pyramidal cells give rise to a beta rhythm, and the cell assemblies are recovered with a temporal separation between cells firing in different cycles. We present experimental evidence showing that such a separation can occur in hippocampal slices.

**Keywords:** gamma rhythms, beta rhythms, cell assembly formation, plasticity, hippocampus, neocortex, preprocessing

### 1. Introduction

Rhythms in the gamma (30–80 Hz) and beta (12–30 Hz) frequency bands have been associated with awareness, perception, and response to novelty (Haenschel et al., 2000; Fries et al., 1997; Fries et al., 2001; Gomez et al.,

1998; Tallon-Baudry and Bertrand, 1999) and (Pearson and Andersen, pers. comm.). It has been suggested that these rhythms are important for “binding” cells within a cell assembly and for facilitating distributed processing in the nervous system (Gray et al., 1989; Gray, 1999; Joliot et al., 1994; Farmer, 1998).

The role of rhythms in the nervous system is still mysterious, and it is even controversial whether rhythms have any functional importance (Shadlen and Movshon, 1999). Though gamma and beta rhythms have been observed to occur together or in succession (Haenschel et al., 2000; Traub et al., 1999a; Gross and Gotman, 1999; Pesaran and Andersen, pers. comm.; Tallon-Baudry et al., 1999), the functional significance of this temporal relationship is an open question. It is also not well understood what role rhythms may play in the creation of cell assemblies (Bibbig, 1999).

Gamma-to-beta transitions have been studied most thoroughly in hippocampal slices (Faulkner et al., 1999; Traub et al., 1999b; Whittington et al., 1997). In slice preparations, tetanic stimulation can produce a spontaneous transition from the gamma rhythm to the beta rhythm. This transition is associated with recovery of ionic currents suppressed by the metabotropic effect of the stimulation and by plastic changes in functional synapses. The differences in currents and functional connectivity underlying the two rhythms lead to differences in temporal structure: in the tetanically produced gamma rhythm, the participating cells fire in every cycle. By contrast, in the beta rhythm, pyramidal cells skip one or more cycles. Since most pyramidal cells skip the same cycles, the local field potential displays a lower frequency.

This article focuses on how networks may create cell assemblies from a weakly structured input. Our simulations show that networks displaying a gamma rhythm are able to create a sharp separation between cells in or out of a cell assembly, while networks displaying a beta rhythm do not have this property. However, networks that display a gamma rhythm followed by a beta rhythm, with plastic changes in synapses during the gamma rhythm, can create a temporal separation of cells in which those within the assembly fire at different times from those outside the assembly. We present experimental results that support this prediction.

We propose that the gamma rhythm can act as a pre-processor for the beta rhythm, allowing networks displaying a beta rhythm to maintain cell assemblies established during the gamma rhythm. It has previously been shown (Ermentrout and Kopell, 1998; Kopell et al., 2000) that the currents and functional connectivity of a network displaying a beta rhythm make it suitable for coordination over longer conduction delays than networks displaying a gamma rhythm. Thus, the gamma and beta rhythms may play complementary roles in processing, with the gamma rhythm preparing

the beta rhythm for participation in long-distance coordination.

## 2. Methods

### 2.1. Computational Methods

Simulations were carried out in a network of pyramidal cells (*E*-cells) and interneurons (*I*-cells). Each cell was modeled as a one-compartment neuron that is coupled to all other neurons in the network. We assumed that all neurons in the network were located within the same local area, so neither spatial organization nor conduction delays were taken into account. The pyramidal cells were made heterogeneous by adding different drives to each cell. Some simulations used an unstructured drive distribution, in which the input to the pyramidal cells varied linearly (uniformly) over some range, as a function of the cell index. Other simulations were done with structure in the drives that mirrored physiologically relevant features. Differential input to neighboring subsets of the population was modeled by a drive depending sigmoidally on the cell index. In this case, there were subsets of cells with weaker and stronger drive, but without a sharp threshold between the subsets. For both types of drives, we assumed that pyramidal cells were located closely enough to share the same pool of interneurons.

Our simulations were carried out in a large network (1,000 pyramidal cells and 300 interneurons), in an intermediate size network with (128 pyramidal cells and 40 interneurons), and in a small network (16 pyramidal cells and 5 interneurons). Excitatory and inhibitory conductances were scaled such that the total synaptic current from each cell remained the same when the population fired synchronously. Such scaling creates a region of phase space for the large network in which the dynamics are expected to be the same as for the smaller networks (which can be considered a lumped version of the large network). In spite of using random initial conditions, we never found behavior for the large network not displayed by the medium-size or small network; in the absence of noise, our simulations gave the same results for all networks. Consequently, our results did not depend on having a large number of cells. Simulations with noise were carried out only for the large network, since the smaller networks have too few cells to allow adequate statistical behavior. All simulations are shown with the large network unless explicitly stated in the figure captions.

The gamma rhythm was modeled using a network of fast-spiking interneurons and pyramidal cells. The currents and synaptic connections were based on studies in hippocampal slices (Traub et al., 1999b; Whittington et al., 1997). The beta rhythm was obtained by activating recurrent excitatory connections and a slow outward afterhyperpolarization current (Kopell et al., 2000; Traub et al., 1999b). This and other slow outward (potassium) currents are suppressed during the gamma rhythm by metabotropic activation resulting from the tetanic stimulation (Whittington et al., 2000). The recurrent excitatory connections activated during the beta rhythm has been shown to potentiate as a result of synchrony during the gamma rhythm (Whittington et al., 1997). As in related earlier work (Kopell et al., 2000), the collection of slow currents was modeled, for simplicity, as a voltage dependent M-current with an appropriate decay time. Such an M-current has been found in both hippocampal slice preparations and in neocortex (Halliwell and Adams, 1982; Halliwell, 1982), along with other slowly decaying potassium currents. However, previous mathematical analysis (Kopell et al., 2000) and related large-scale simulations (Traub et al., 1996a; Traub et al., 1999b) suggest that other details are not critical to the gamma and beta network oscillations seen experimentally.

Interneurons and pyramidal cells were modeled by the Hodgkin-Huxley Eqs. (1) and (2) (Hodgkin and Huxley, 1952). Both types of neurons were given basic sodium (Na) and potassium (K) spiking currents, a leak current (L), and an applied current (Appl). These are the only currents required to obtain a gamma rhythm. During the gamma rhythm there were active  $E-I$ ,  $I-I$ , and  $I-E$  synaptic connections. To get the gamma to beta transition, the M-current (M) and recurrent excitatory ( $E-E$ ) connections were activated in the pyramidal cells. During the gamma to beta transition, the activation was ramped up linearly from zero over a fixed interval of time (from 100 to 200 ms), mimicking the recovery of the M-current from metabotropic suppression and the potentiation of recurrent excitation during the gamma period. The applied current to the pyramidal cells was given a range of values varying almost twofold (from 4.25 to 8.0  $\mu\text{A}/\text{cm}^2$ ), while the applied current to the interneurons was constant (1.3  $\mu\text{A}/\text{cm}^2$ ). The sigmoidal distribution of the applied current was modeled as

$$I = \frac{I_{mi} - I_{ma}}{1 + \alpha \left(\frac{i-1}{NE/2}\right)^r} + I_{mi},$$

where  $I_{mi} = 4.25$  and  $\mu\text{A}/\text{cm}^2$ ,  $I_{ma} = 8.0$   $\mu\text{A}/\text{cm}^2$  were the minimal and maximal input currents,  $NE$  was the number of pyramidal cells,  $i = 0, 1, \dots, NE - 1$ ,  $r = 2, 4, 7$ ,  $\alpha = (I_{mi} - a)/(a - I_{ma})$ , where  $a = c(I_{mi} + I_{ma})$ , and  $c$  was chosen such that the mean drive remained fixed at 6.125  $\mu\text{A}/\text{cm}^2$ . For the sigmoids in Fig. 6A,  $c = 0.494, 0.552, 0.582$ . The linear drive distribution followed the cell index—that is,

$$I = i \frac{I_{ma} - I_{mi}}{NE - 1} + I_{mi},$$

where  $i = 0, 1, \dots, NE - 1$  is the cell index. The applied current to the interneurons was constant (1.3  $\mu\text{A}/\text{cm}^2$ ); hence they can be lumped into a single unit. The excitatory synapses were modeled as AMPA-mediated, and the inhibitory synapses were modeled as GABA<sub>A</sub> mediated.

For the pyramidal cells, the current balance equation is

$$\begin{aligned} c \frac{dv_j}{dt} = & -[g_{Na} h_j m_j^3 (v_j - E_{Na}) + g_K n_j^4 (v_j - E_K) \\ & + g_M w_j (v_j - E_M) + g_L (v_j - E_L) \\ & + g_{IE} (s_{IE})_j (v_j - E_{IE}) \\ & + g_{EE} (s_{EE})_j (v_j - E_{EE})] + I_{Appl}, \end{aligned} \quad (1)$$

where  $j = 0, \dots, NE$ ,  $v_j$  is the voltage,  $c$  is the membrane capacity (1  $\mu\text{F}$ ),  $E_{IE}$  and  $E_{EE}$  are the reversal potentials, and  $I_{Appl}$  is the applied current. The variables  $g_{Na}$ ,  $g_K$ ,  $g_M$ , and  $g_L$  are the maximal ionic conductances, and the variables  $h$ ,  $m$ ,  $n$ , and  $w$  represent the gating of the channels. The variables  $g_{IE}$  and  $g_{EE}$  are the maximal synaptic conductances, while  $s_{IE}$  and  $s_{EE}$  represent the synaptic kinetics of the  $I-E$  and  $E-E$  connections.

For the interneurons, the current balance equation is

$$\begin{aligned} c \frac{dv_j}{dt} = & -[g_{Na} h_j m_j^3 (v_j - E_{Na}) + g_K n_j^4 (v_j - E_K) \\ & + g_L (v_j - E_L) + g_{II} (s_{II})_j (v_j - E_{II}) \\ & + g_{EI} (s_{EI})_j (v_j - E_{EI})] + I_{Appl}, \end{aligned} \quad (2)$$

where  $j = 0, \dots, NI$  and  $NI$  is the number of interneurons. The variables representing the voltage, reversal potentials, and ionic and applied currents are the same as above. The variables  $g_{EI}$  and  $g_{II}$  are the maximal conductances, and the variables  $s_{EI}$  and  $s_{II}$  represent the synaptic kinetics of the  $E-I$  and  $I-I$  connections.

The gating equations are

$$\frac{dx_j}{dt} = a_x(v_j)(1 - x_j) - b_x(v_j)x_j,$$

where  $x = m, h, n$ . For the M-current, the gating equation is

$$\frac{dw_j}{dt} = \frac{w_\infty - w_j(v_j)}{\tau(v_j)}.$$

The synaptic kinetics are described by

$$(S_{EE})_j = \sum_{k=0}^{NE-1} S_{E_k E_j}, \quad (S_{IE})_j = \sum_{k=0}^{NI-1} S_{I_k E_j},$$

$$(S_{EI})_j = \sum_{k=0}^{NE-1} S_{E_k I_j}, \quad (S_{II})_j = \sum_{k=0}^{NI-1} S_{I_k I_j},$$

where

$$\frac{ds_{E_k R_j}}{dt} = g_E(v_j)(1 - s_{E_k R_j}) - \frac{s_{E_k R_j}}{\tau_1}, \quad (3)$$

$$\frac{ds_{I_k R_j}}{dt} = g_I(v_k)(1 - s_{I_k R_j}) - \frac{s_{I_k R_j}}{\tau_2}, \quad (4)$$

and  $\tau_1 = 2$ ,  $\tau_2 = 10$ .

Equation (3) describes synapses from  $E$ -cell  $k$  to  $R_j = E_j, I_j$  depending on the postsynaptic cell, while Eq. (4) describes synapses from  $I$ -cell  $k$  to  $R_j = E_j, I_j$ . Finally,

$$a_m(v_j) = \frac{0.32(v_j + 54)}{1 - \exp(-(v_j + 54)/4)},$$

$$b_m(v_j) = \frac{0.28(v_j + 27)}{\exp((v_j + 27)/5) - 1},$$

$$a_h(v_j) = 0.128 \exp(-(v_j + 50)/18),$$

$$b_h(v_j) = \frac{4}{1 + \exp(-(v_j + 27)/5)},$$

$$a_n(v_j) = \frac{0.032(v_j + 52)}{1 - \exp(-(v_j + 52)/5)},$$

$$b_n(v_j) = 0.5 \exp(-(v_j + 57)/40),$$

$$w_\infty(v_j) = \frac{1}{1 + \exp(-(v_j + 35)/10)},$$

$$\tau(v_j) = \frac{400}{3.3 \exp((v_j + 35)/20) + \exp(-(v_j + 35)/20)},$$

and

$$g_E(v_j) = 5(1 + \tanh(v_j/4)),$$

$$g_I(v_j) = 2(1 + \tanh(v_j/4)).$$

The total synaptic strength was kept constant as the network size was changed by normalizing the individual synaptic conductances relative to the size of the network. Connections originating from the pyramidal cells were scaled by the total number of presynaptic pyramidal cells participating in the connection and connections originating from the interneurons were scaled by the number of interneurons. The total intrinsic and synaptic conductances and reversal potentials for all ions and synapses are shown in Table 1. The kinetics of the M-current is based on earlier work by Crook et al. (1997, 1998), and the remaining equations and parameters are from Ermentrout and Kopell (1998).

To verify the robustness of our simulations, white noise was added independently to the applied currents of all pyramidal cells and interneurons. Each noisy applied current had the form

$$I_{Appl_n} = I_{Appl} + \sigma \eta(t).$$

Here  $I_{Appl}$  is the time-independent input from Eqs. (1) and (2),  $\eta(t)$  is the noise spread, chosen as a Gaussian-distributed random sequence with zero mean and unit half-width, and  $\sigma = \sigma_0 \sqrt{\Delta t}$ , where  $\sigma_0$  is a constant noise amplitude and  $\Delta t$  is the integration step-size. The noise amplitudes were chosen as  $\sigma = 2, 4, 6 \mu\text{A}/\text{cm}^2$ .  $\sigma = 2$  represents the scaled network with a low level of noise about half the spread in the excitatory drive,  $\sigma = 4 \mu\text{A}/\text{cm}^2$  represents a noise level that is comparable to the spread in the excitatory drive, and

*Table 1.* Maximal conductances ( $\text{mS}/\text{cm}^2$ ) and reversal potentials for the intrinsic and synaptic currents within each cell. The total synaptic conductance is the sum of all the synaptic conductances from a given cell; e.g., in a network with five  $I$ -cells, the maximal conductance from each  $I$ -cell to any  $E$ -cell will be  $g_{IE} = 1.00/5 \text{ mS}/\text{cm}^2$ .

Intrinsic		Synaptic					
Conductance $\text{mS}/\text{cm}^2$	Reversal potential mV	Total conductance $\text{mS}/\text{cm}^2$	Reversal potential mV				
$g_{Na}$	100.0	$E_{Na}$	50	$g_{IE}$	1.00	$E_{IE}$	-80
$g_K$	80.0	$E_K$	-100	$g_{EE}$	0.50	$E_{EE}$	0
$g_M$	1.0	$E_M$	-100	$g_{II}$	0.25	$E_{II}$	-80
$g_L$	0.1	$E_L$	-67	$g_{EI}$	0.30	$E_{EI}$	0

$\sigma = 6 \mu A/cm^2$  represents a noise level that is approximately 1.5 times the spread in the excitatory drive. Note that in this noisy simulation, the interneurons received independent noisy perturbations and hence could not be lumped into a single unit. As mentioned earlier, these simulations were done only with the large network.

All simulations were carried out on Unix workstations, using a C/C++ implementation of the fourth-order Runge-Kutta method for solving the Hodgkin-Huxley equations.

## 2.2. Experimental Methods

Transverse hippocampal slices (450 micrometers thick) were prepared from male Sprague-Dawley rats (200–250 g) following anesthesia (enflurane) and cervical dislocation. Slices were maintained in an interface chamber and perfused with artificial cerebrospinal fluid (ACSF) containing (in mM): NaCl 135,  $NaHCO_3$  18, KCl 3,  $CaCl_2$  2,  $NaH_2PO_4$  1.25,  $MgCl_2$  1, D-Glucose 10, equilibrated with 95% $O_2$ /5% $CO_2$  pH 7.2 at 33–35 C. Oscillations were generated by paired tetanic stimuli (8 pulses at 100 Hz, 30–50 V) delivered to two sites in distal stratum radiatum separated by 0.7–1 mm. (For such a separation, conductance delays are at most a few ms.) Stratum pyramidale field potentials were recorded with glass micropipettes filled with 2 M NaCl with the same range of distances between recording sites as above. Note that the distance between sites in the present experiments is smaller than that used previously to examine “long-range” synchrony (e.g., Whittington et al., 1995), as both populations of pyramidal cells needed to be driven by a synchronous, inhibition-based oscillation. Pairs of posttetanic oscillations were recorded from area CA1 in five slices. In each case, following control recordings, the degree of excitability of one site was weakened immediately following the tetanic stimulation by pressure ejection of ACSF with composition as above but with no potassium ions present.

## 3. Results

### 3.1. Gamma and Beta Rhythms: Creation, Modulation, and Temporal Separation of Thresholds

We present two principal results. First, in a network with heterogeneous drive to the pyramidal cells and parameters appropriate to displaying a gamma rhythm, pyramidal cells are partitioned into two groups—those

that are participating in a nearly synchronous cell assembly and those that are completely suppressed (see Traub et al., 1997), for related work on suppression of pyramidal cells). We show that such a partition does not occur if the network has parameters appropriate for displaying a beta rhythm.

Second, a network displaying a beta rhythm is able to create a temporal separation between the two groups obtained during the gamma rhythm. This separation requires Hebbian preprocessing during a prior interval in which the network displays a gamma rhythm. We adopt the hypothesis that pyramidal cells exhibit short-term plasticity that strengthens recurrent excitation among cells participating in the gamma rhythm and weakens synapses to the interneurons from the cells suppressed during the gamma rhythm. Experimental evidence related to this hypothesis can be found in Traub et al. (1999b) and Whittington et al. (1997). Fig. 1A shows the network displaying the participating and suppressed cells and Fig. 1B shows the network after Hebbian modification.

During the beta rhythm, those pyramidal cells with a drive above some threshold fire together in the same cycles of the interneuronal rhythm, while the less activated cells fire less often and in cycles missed by the more activated cells. This temporal separation occurs even in the presence of significant levels of noise. It is based on subtle points of timing of the interneurons, and in the next section we give an explanation of how it works.

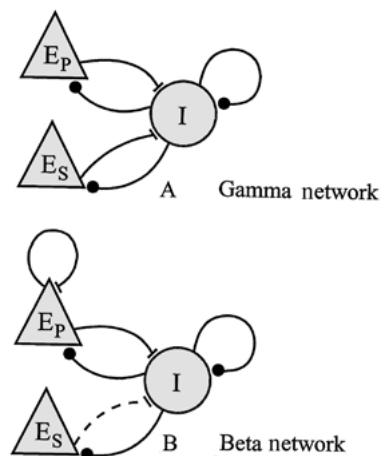


Figure 1. A diagram the partition of  $E$ -cells into two groups during the gamma rhythm—participating cells ( $E_P$ ) and suppressed cells ( $E_S$ ). B shows the synaptic modifications that lead to the temporal separation between the two groups during beta. Recurrent excitatory connections are activated among the  $E_P$ -cells and the  $E_S$ - $I$  connections (dashed line) are weakened.

The most obvious prediction from our modeling is that, during the beta rhythm, the more activated cells produce a field potential whose peaks differ from those of the less activated cells by a multiple of a gamma period. This can be tested experimentally, and we present results showing that such a separation can occur in the hippocampus.

### 3.1.1. Networks Displaying a Gamma Rhythm Create Thresholds for Participation in Cell Assemblies.

Figure 2 illustrates the basic threshold phenomenon, using an applied current from 4.25 to 8.00  $\mu\text{A}/\text{cm}^2$  increasing uniformly with the cell index. The pyramidal cells with the strongest drive participate in a gamma rhythm, spiking once on every cycle with a frequency of 71 Hz. We designate these cells participating cells ( $E_P$ -cells). The pyramidal cells with a weaker drive are suppressed and these we designate  $E_S$ -cells. Finally, a very small number of cells (less than 5%) are partially suppressed.

The boundary between the  $E_P$ - and the  $E_S$ -cells can be modulated by changing the average applied current to either the interneurons or the pyramidal cells. Increasing the applied current to the interneurons by 100% (from 1.0 to 2.0  $\mu\text{A}/\text{cm}^2$ ) increases the number of suppressed cells from 33% to 48% (for a simulation with 128  $E$ -cells, see Table 2), and increasing the mean applied current to the  $E$ -cells by 100% (from 3.75–7.5  $\mu\text{A}/\text{cm}^2$ ) decreases the number of suppressed cells from 53% to 33% (again for a simulation with 128  $E$ -cells, see Table 3). Similar effects can be obtained by changing synaptic conductances (see Tables 2 and 3). For example, increasing the  $I$ - $I$  conductance effectively decreases the drive to the  $I$ -cells and hence the number of suppressed cells. An explanation of these phenomena is given in the section on timing.

Changing the relative amount of *heterogeneity* of the drive (keeping the mean drive constant but varying the upper and lower bounds of the drive) also modulates the proportion of  $E_P$ - and  $E_S$ -cells. In a network with low levels of heterogeneity, all pyramidal cells fire in every cycle. Adding heterogeneity using uniformly spread drives but keeping the mean drive fixed increases the frequency and separates the pyramidal cells into the two groups ( $E_P$  and  $E_S$ ) with the boundary dependent on the amount of heterogeneity (data not shown).

### 3.1.2. Activating the M-Current Destroys Threshold.

Figure 3A shows the firing of the pyramidal cells when

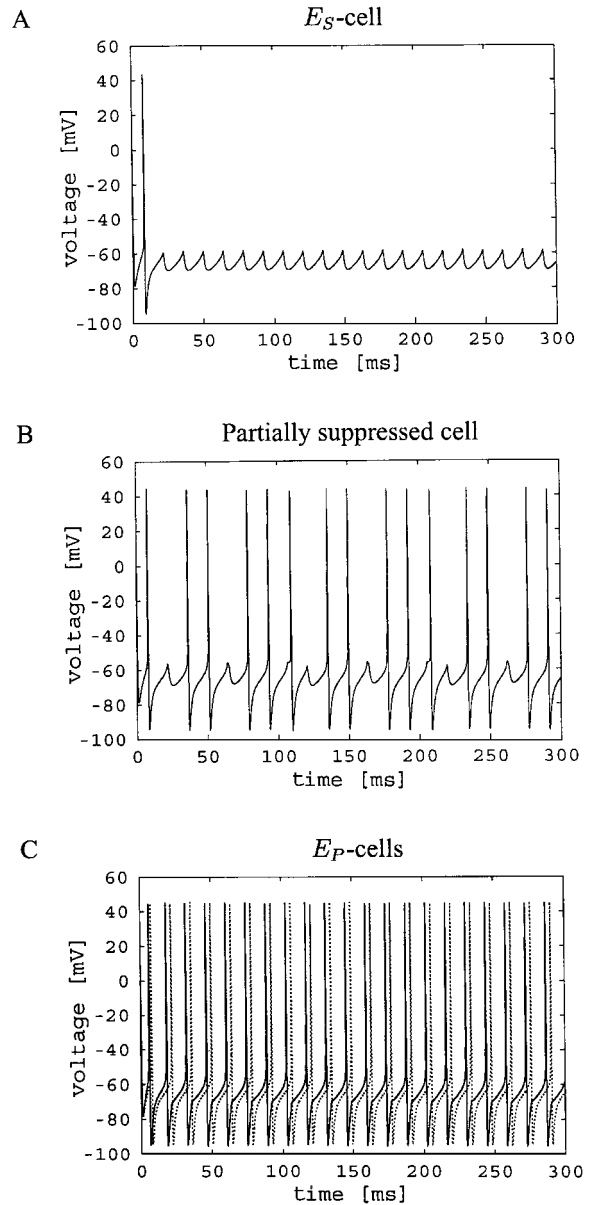


Figure 2. Partition of the network into participating cells ( $E_P$ -cells) and suppressed cells ( $E_S$ -cells). A shows a suppressed cell, B shows a partially suppressed cell, and C shows two participating cells that fire in every cycle. Note that there is a 4 ms delay between the onset of firing of the strongest and weakest driven  $E_P$ -cells (denoted by a solid and a dotted line) in C. The firing frequency of the interneurons and the  $E_P$ -cells is 71 Hz.

the slow outward M-current is added, ramped up linearly during 100 ms (from 100 to 200 ms). For the  $E_S$ -cells, there is no activity during the gamma rhythm (from 0 to 100 ms) while the  $E_P$ -cells fire in every cycle. During the transition from the gamma to the beta

*Table 2.* Parameter variations for input to the  $I$ -cells in the gamma regime. The data shown in the table are for a network with 128  $E$ -cells and 40  $I$ -cells. The table shows that increasing the excitation to the interneurons (increasing the drive to the  $I$ -cells, the  $E-I$  coupling, or decreasing the  $I-I$  coupling) leads to higher frequencies and more suppressed cells. The first column displays effects of modulation of tonic drive to  $I$ -cells, the second, excitatory drive to  $I$ -cells, and the third inhibitory drive to  $I$ -cells.

Tonic drive to $I$ -cells					Excitatory synaptic drive to $I$ -cells					Inhibitory synaptic drive to $I$ -cells				
$I$ -drive	Frequency	$E_S$ -cells (%)	$E_{PS}$ -cells (%)	$E_P$ -cells (%)	$E-I$	Frequency	$E_S$ -cells (%)	$E_{PS}$ -cells (%)	$E_P$ -cells (%)	$I-I$	Frequency	$E_S$ -cells (%)	$E_{PS}$ -cells (%)	$E_P$ -cells (%)
0.0	63.0	18.0	1.6	80.4	0.1	58.8	7.0	0.8	92.2	0.0	72.7	43.0	3.1	53.9
0.2	64.1	21.1	1.6	77.3	<b>0.3</b>	<b>70.4</b>	<b>37.5</b>	<b>2.3</b>	<b>60.2</b>	0.1	73.2	43.8	3.1	53.1
0.4	65.3	24.2	1.6	74.2	0.5	75.0	48.4	3.1	48.5	<b>0.3</b>	<b>70.4</b>	<b>37.5</b>	<b>2.3</b>	<b>60.2</b>
0.6	66.4	27.3	1.6	71.1	0.7	77.6	54.7	3.9	41.4	0.4	68.0	31.3	1.6	67.2
0.8	67.5	30.4	1.6	68.0	0.9	79.5	59.4	4.7	35.9	0.6	65.1	23.4	1.6	75.0
1.0	68.7	32.8	2.3	64.9	1.1	80.1	60.2	4.7	35.1	0.8	62.5	16.4	1.6	82.0
1.2	69.8	35.9	2.3	61.8										
<b>1.3</b>	<b>70.4</b>	<b>37.5</b>	<b>2.3</b>	<b>60.2</b>										
1.4	71.0	39.1	1.6	59.3										
1.6	72.2	41.4	2.3	56.3										
1.8	73.2	44.5	2.3	53.2										
2.0	74.6	47.7	3.1	49.2										
2.2	76.0	50.8	3.1	46.1										
2.4	77.5	53.9	4.7	41.4										

*Table 3.* Parameter variations for input to the  $E$ -cells in the gamma regime. The data shown in the table are for a network with 128  $E$ -cells and 40  $I$ -cells. The table shows that increasing the excitation to the pyramidal cells (increasing the drive to the  $E$ -cells or decreasing the  $I-E$  coupling) leads to higher frequencies but fewer suppressed cells.

Tonic drive to $E$ -cells					Inhibitory synaptic drive to $E$ -cells				
$E$ -drive	Frequency	$E_S$ -cells (%)	$E_{PS}$ -cells (%)	$E_P$ -cells (%)	$I-E$	Frequency	$E_S$ -cells (%)	$E_{PS}$ -cells (%)	$E_P$ -cells (%)
4.125	55.2	50.8	0.8	48.4	0.6	93.7	15.6	3.1	81.3
4.875	61.0	46.2	0.8	53.0	0.8	79.8	29.7	2.3	68.0
5.625	66.9	41.4	1.6	57.0	<b>1.0</b>	<b>70.4</b>	<b>37.5</b>	<b>2.3</b>	<b>60.2</b>
<b>6.125</b>	<b>70.4</b>	<b>37.5</b>	<b>2.3</b>	<b>60.2</b>	1.2	63.9	41.4	1.6	57.0
6.375	72.8	38.2	1.6	60.2	1.4	59.2	44.5	1.6	53.9
7.125	78.6	34.4	3.1	62.5	1.6	55.6	46.8	1.6	51.6
7.875	84.6	31.3	3.9	64.8	1.8	52.8	50.0	0.8	49.2
8.625	90.6	28.9	3.9	67.2	2.0	50.6	52.3	0.0	47.7

rhythm (from 100 to 200 ms), the activity of the  $E$ -cells almost disappears. This phenomenon has also been observed in experiments in hippocampal CA1 (Faulkner et al., 1999). After the M-current is ramped up, both  $E_P$ - and  $E_S$ -cells fire with frequencies in the beta range. Note that adding the slow outward current allows pyramidal cells suppressed during the gamma rhythm to fire occasionally. Each cell fires during a fraction of the cycles, but the cells do not all fire on the same subharmonics of the interneuronal rhythm. Neverthe-

less, on every cycle a significant fraction of the cells fire. The population therefore displays a gamma rhythm (see Fig. 3B). Thus, there is no well-defined cell assembly once the adaptation current is involved, and there is also no population beta rhythm.

### 3.1.3. Activating the M-Current and Recurrent Excitatory Connections Creates a Beta Rhythm.

The excitatory postsynaptic potentials (EPSPs) that are observed in pyramidal cells during the beta rhythm

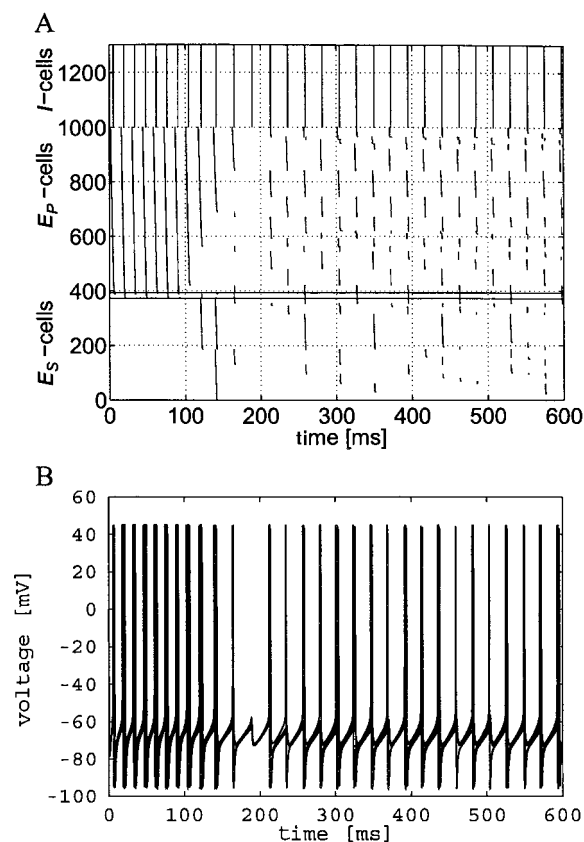


Figure 3. When the M-current is added to the pyramidal cells (ramped up from 100 to 200 ms) the network exhibits a population gamma rhythm. A shows the cycles on which the pyramidal cells fire. This is shown as a raster plot of  $E$ -cells (cells 0 to 1000) and  $I$ -cells (cells 1000 to 1300) activity as a function of time. The  $E$ -cells are labeled with increasing drive, such that  $E$ -cell 0 has the lowest drive and  $E$ -cell 1000 has the highest drive. Since this simulation does not include noise, the  $I$ -cells all have the same drive so the labeling for these cells has no significance. The same organization has been used in Figs. 4–9. The  $E$ -cells are partitioned into  $E_S$ -cells (0 to 323), partially suppressed cells (324 to 400), the cells between the two horizontal lines), and  $E_P$ -cells (401 to 1000). B shows the population gamma rhythm. This graph is obtained by superimposing the activity of the  $E_P$ -cells. Note that the frequency of the population gamma rhythm (as seen in B and by the frequency of the  $E_P$ -cells) decreases from 71 Hz to 44 Hz when the M-current is added.

are believed to depend on prior synchrony during the gamma rhythm; manipulations that reduce this synchrony also reduce or destroy the formation of the EPSPs (Faulkner et al., 1999; Traub et al., 1999b; Whittington et al., 1997). Thus, it is reasonable to hypothesize that only those pyramidal cells that participate in the gamma rhythm exhibit increases in the strength of their mutually excitatory synapses.

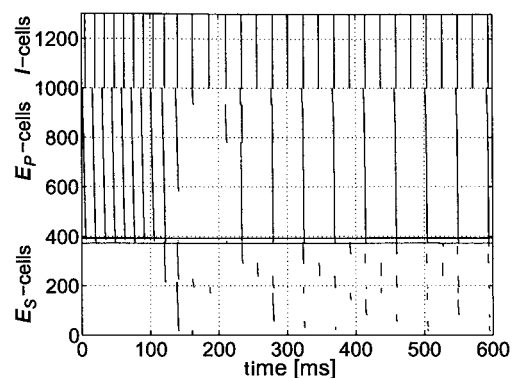


Figure 4. When recurrent excitatory connections among  $E_P$ -cells are added, the network displays a beat-skipping beta rhythm with a weak temporal separation between  $E_P$ - and  $E_S$ -cells.

Figure 4 shows that a population beta rhythm with a weak temporal separation is obtained by simultaneously ramping up the M-current and recurrent excitatory connections among the  $E_P$ -cells. Activating connections only among the  $E_P$ -cells results in a beat-skipping beta rhythm; the  $E_P$ -cells fire synchronously on every other cycle, whereas the  $E_S$ -cells fire much more infrequently and irregularly. Some of the active  $E_S$ -cells show a preference for firing in antiphase to the beat-skipping beta rhythm, thus creating a weak temporal separation between  $E_P$ - and  $E_S$ -cells.

The restriction of  $E$ - $E$  connections to  $E_P$ -cells is crucial. If recurrent excitatory connections are added among *all* pyramidal cells, both  $E_S$ -cells and  $E_P$ -cells fire in a beat-skipping beta rhythm, with all cells firing on the same cycles of the interneuronal rhythm (data not shown).

### 3.1.4. Further Hebbian Modifications Create a Temporal Separation Between $E_P$ - and $E_S$ -Cells.

Activation of recurrent excitatory connections among  $E_P$ -cells along with Hebbian modification of the  $E_S$ - $I$  connections gives the network shown in Fig. 1B. The latter modification used in this article is a decrease in conductance of the  $E$ - $I$  synapses from the  $E_S$ -cells to the interneurons, while the  $E$ - $I$  conductances from the  $E_P$ -cells is kept constant. This change results in well-defined cell assemblies in which the  $E_P$ -cells display a beat-skipping beta rhythm and the  $E_S$ -cells fire mainly in antiphase to the beat-skipping rhythm (see Fig. 5A):  $E_S$ -cells with a weaker drive are more likely to fire in antiphase, while  $E_S$ -cells close to the  $E_P$ -cell boundary

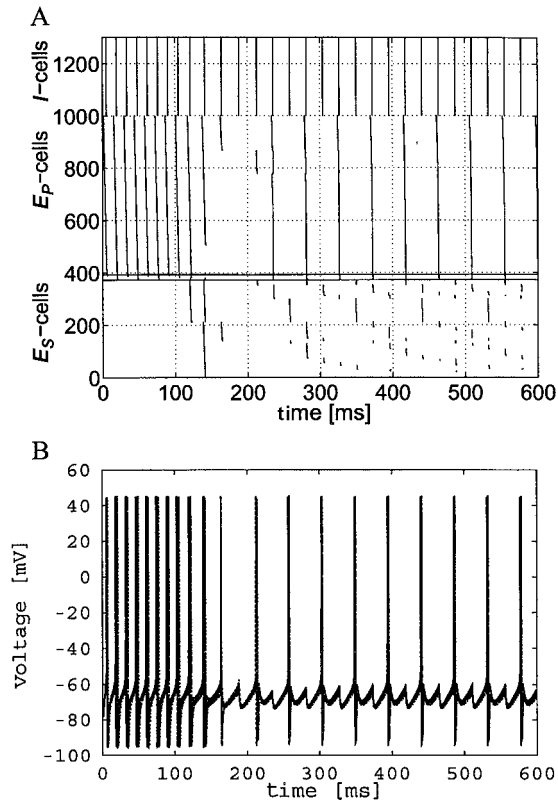


Figure 5. When recurrent excitation is introduced only among  $E_P$ -cells and the  $E_S$ - $I$  connections are weakened, the network displays a somewhat better temporal separation, with the  $E_P$ -cells displaying a beat-skipping beta rhythm and the  $E_S$ -cells firing preferentially during off-beat cycles. A shows the cycles on which pyramidal cells and interneurons fire and B shows a superposition of the firing  $E_P$ -cells.

sometimes fire during the same cycles as the  $E_P$ -cells. Note that  $E_S$ -cells fire less frequently than the  $E_P$ -cells, so that a model field potential reflecting the activity of the former would be smaller than one reflecting the activity of the latter. Comparing the results in Figs. 4 and 5A shows that reducing the  $E_S$ - $I$  connections creates a better separation. Without the reduction of the  $E_S$ - $I$  connections (see Fig. 4), approximately 50% of the  $E_S$ -cells fire in antiphase with the  $E_P$ -cells, while after the reduction approximately 85% fire in antiphase with the  $E_P$ -cells.

Note also that the synchrony of the beta rhythm is more precise than that of the gamma rhythm both in experiments (Faulkner et al., 1999; Whittington et al., 1997) and in our model. During the gamma rhythm, our model has a 4 ms delay (see Fig. 2) between firing of the  $E_P$ -cell with the strongest drive and the one with

the weakest drive, but during the beta rhythm that delay is reduced to 1.85 ms. Figure 5B displays the firing of the  $E_P$ -cells.

Changing the  $I$ - $E$  synaptic strength does not significantly change the ability of the network to create thresholds during the beta rhythm (data not shown). Similarly, changing the  $E$ - $I$  conductance uniformly for all the pyramidal cells does not help to create a threshold (data not shown).

All of the previous simulations used an applied current to the pyramidal cells that varied uniformly among the cells. If the drive is changed to vary sigmoidally, and hence some structure is added to the input, even a relatively small departure from uniform variance (e.g., sig 1 in Fig. 6) leads to a sharp threshold with *all*  $E_S$ -cells firing in antiphase to the  $E_P$ -cells. With a large sigmoidal bias (sig 3 in Fig. 6), it is no longer necessary to weaken  $E_S$ - $I$  in order to obtain a temporal separation during the beta rhythm, compare panels E and F in Fig. 6F.

Changing the mean drive either by shifting the sigmoids up or down (data not shown) or left and right (see Fig. 7) does not significantly affect the network's ability to create well-defined temporal cell assemblies. Increasing the mean drive from  $5.887 \mu\text{A}/\text{cm}^2$  to  $6.215 \mu\text{A}/\text{cm}^2$  (Fig. 7, panels B and C) increases the number of  $E_P$ -cells by 65, while decreasing the mean drive from  $5.887 \mu\text{A}/\text{cm}^2$  to  $5.574 \mu\text{A}/\text{cm}^2$  (Fig. 7, panels B and D) decreases the number of  $E_P$ -cells by 59. If the sigmoids are shifted up by a constant (of approximately  $0.5 \mu\text{A}/\text{cm}^2$ ) such that the maximum drive becomes  $8.5 \mu\text{A}/\text{cm}^2$  and the minimum drive becomes  $4.75 \mu\text{A}/\text{cm}^2$ , the firing pattern changes, and  $E_P$ -cells with higher drives start to fire on every cycle of the underlying interneuronal rhythm. Similarly, if the drives are shifted down by the same amount, the  $E_S$ -cells will remain suppressed during beta (instead of firing in antiphase with the  $E_P$ -cells).

Other parameter changes modifying the excitatory input to the  $E$ -cells (e.g., increasing the  $E$ - $E$  coupling or decreasing the  $I$ - $E$  coupling) give similar results. In summary, the above results show that changing the mean of the drive to the  $E$ -cells modulates the limit between participating and suppressed cells, while introducing a sigmoidal bias increases the network's ability to form a temporal separation. The reason that the sigmoids result in a better temporal separation is explained in the section on how the temporal separation work.

As for the gamma simulations, we also need to study the effect of changing the input to the  $I$ -cells. This can

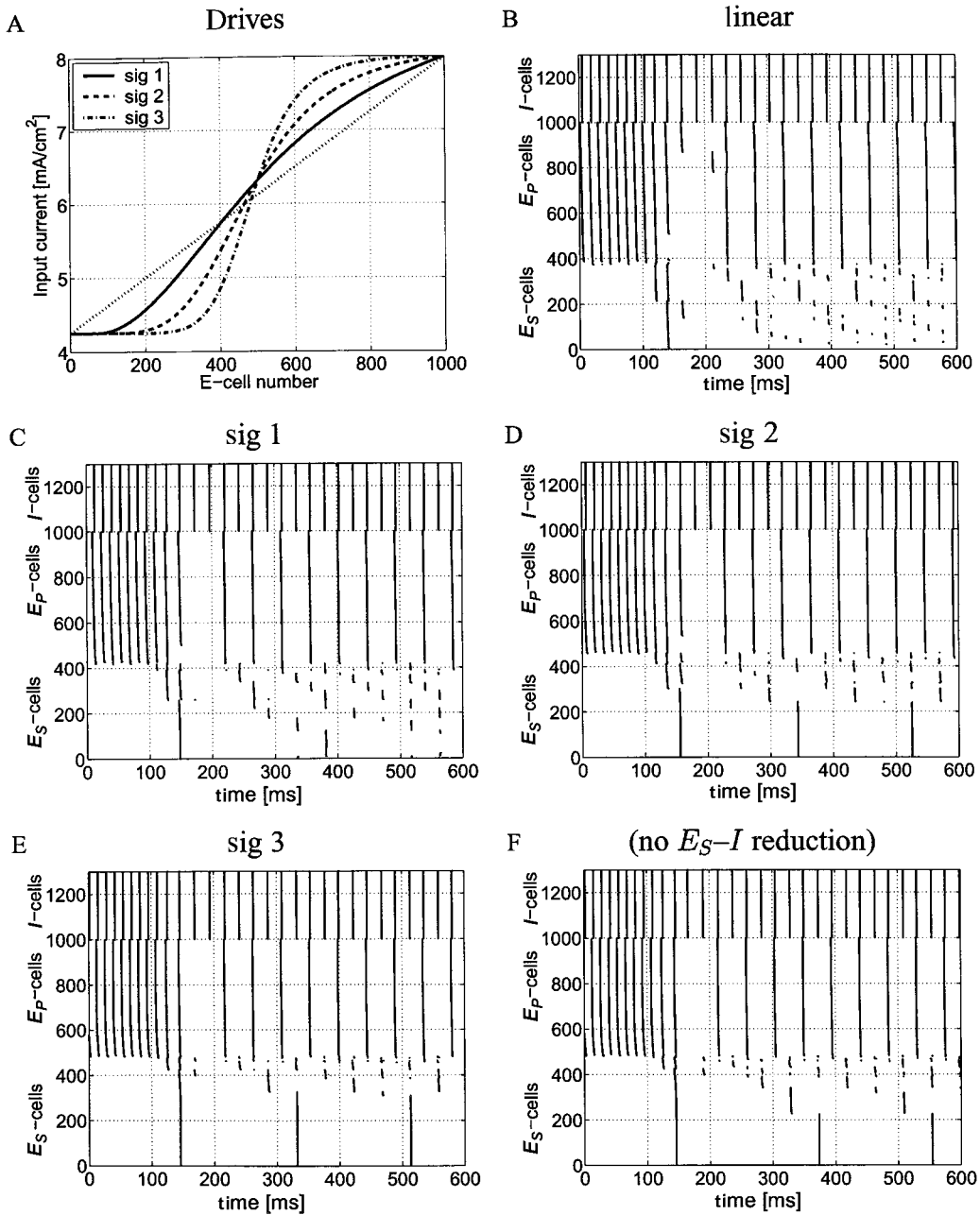


*Figure 6.* When the distribution of drives applied to the pyramidal cells is changed from linear to sigmoidal, the threshold between  $E_P$ - and  $E_S$ -cells is sharpened. Panels B to F show the behavior of the network using the drives shown in panel A. Note that even a mild sigmoidal bias (sig 1) leads to an almost perfect temporal separation. In addition, note that for the strong sigmoid (sig 3) it is *not* necessary to reduce  $E_S$ -I coupling to get a perfect temporal separation.

be done either by changing the drive to the  $I$ -cells or by changing the  $I$ - $I$  or the  $E$ - $I$  coupling strength. As in gamma, we see the same result for either of these changes. Therefore, we have shown only the effect of changing the drive to the  $I$ -cells.

In Fig. 8, we show that increasing the  $I$ -cell drive from  $1.3 \mu\text{A}/\text{cm}^2$  (panel B) to  $1.45 \mu\text{A}/\text{cm}^2$  (panel C) increases the amount of inhibition in the network, and as a result fewer  $E_S$ -cells are able to fire. However, the high level of inhibition makes the  $E_S$ -cells fire during

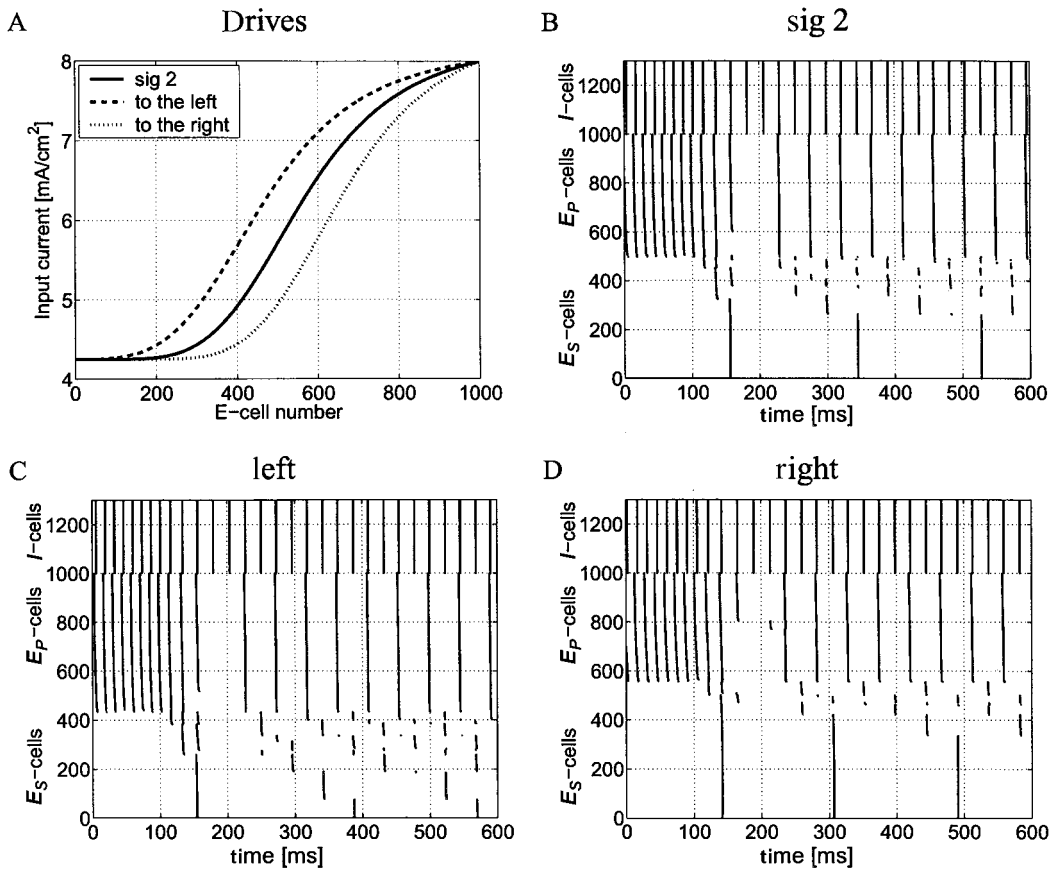


Figure 7. When the mean drive is changed by changing the sigmoids to the left and right, the number of suppressed cells is changed. An increased mean drive (panel C) results in fewer suppressed cells while a decreased mean drive (panel D) results in more suppressed cells. The sigmoid (sig 2) shown on this figure is the same as the one shown in Fig. 6.

the same cycles as the  $E_P$ -cells. The reason for this is explained in the section on how the temporal separation work. If instead the  $I$ -cell drive is decreased from  $1.30 \mu A/cm^2$  (panel B) to  $1.15 \mu A/cm^2$  (panel A), more  $E_S$ -cells are able to fire. The decreased amount of inhibition also affects the firing of the  $E_P$ -cells such that the highest driven cells fire on almost every cycle. For both increased and decreased drive to the  $I$ -cells, there is separation between participating and suppressed cells.

### 3.1.5. The Temporal Separation is Robust to Noise.

The addition of noise leads to minor changes in the network behavior. In the simulation shown in Fig. 9, the average frequency of the interneurons is essentially the same, but there is an increase in the number of partially suppressed pyramidal cells. These results are easy to explain. If a given  $E$ -cell has a nonnoisy input below or

close to the threshold, noise allows it to reach threshold occasionally, thus firing when it would not fire under nonnoisy conditions. This changes some suppressed cells into partially suppressed ones, thus increasing the number of the latter. Similarly, a participating cell close to threshold may sometimes be suppressed by the noise, decreasing the number of  $E_P$ -cells and thus further increasing the number of partially suppressed cells.

Figure 9 shows that, at all levels of noise, a temporal separation is created, as in the nonnoisy case. However, the noise does have some effect on the firing patterns. Adding a moderate amount of noise spreads out the firing of the  $I$ -cells, but the  $E$ -cells keep firing mainly during the off-beat cycles (compare top and middle rows on Fig. 9). At the highest level of noise ( $\sigma = 6 \mu A/cm^2$ ) (bottom row on Fig. 9), the interneurons are less coherent but still exhibit a distinct gamma

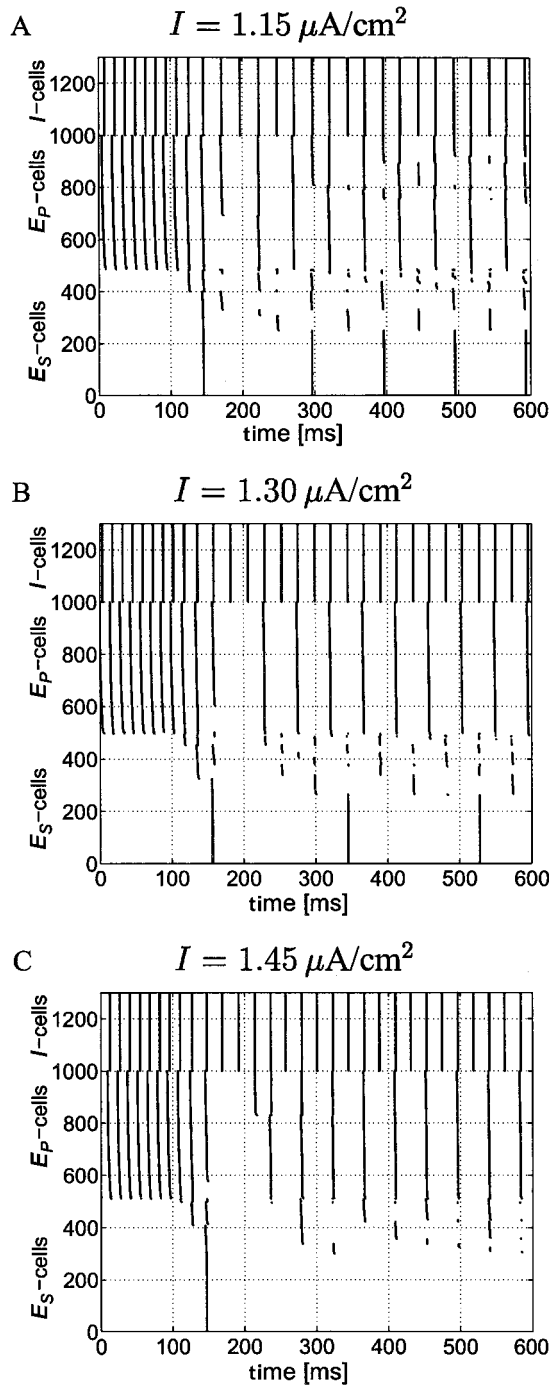


*Figure 8.* When the inhibition is increased by increasing the drive to the  $I$ -cells is changed from  $1.15$  to  $1.45 \mu\text{A}/\text{cm}^2$ , the firing rate of the pyramidal cells is decreased but the separation between participating and suppressed pyramidal cells remain almost constant. When the inhibition is too small, some of the highest driven pyramidal cells fire on every cycle (panel A), while a high inhibition leads to almost total suppression of the  $E_S$ -cells (panel C).

rhythm, sharper during cycles where the  $E_P$ -cells fire. The number of gamma cycles missed by the pyramidal cells is larger for  $\sigma = 6 \mu\text{A}/\text{cm}^2$  than for  $\sigma = 4 \mu\text{A}/\text{cm}^2$ , and the  $E_S$ -cells with the lowest drive are suppressed during the beta rhythm for  $\sigma = 6 \mu\text{A}/\text{cm}^2$ . Finally, the left column of Fig. 9 shows that a high level of noise ( $\sigma = 6 \mu\text{A}/\text{cm}^2$ ) can actually improve temporal separation, even with a uniformly varying (unstructured) drive. More specifically, we note that high levels of noise appear to suppress many of the  $E_S$ -cells that participated during the beta rhythm under nonnoisy conditions. This effect seems to be more pronounced for cells firing on the same cycles as the  $E_P$ -cells, so the global result is a more perfect temporal separation. Finally, note that even though noise is added both during the gamma and the beta rhythms, the noise mainly affects the network's behavior during the beta rhythm, while the behavior during gamma is almost unchanged. A heuristic explanation of effects of noise is included in the discussion.

In summary, we found that the network behavior is robust to the addition of noise. The interneurons become less synchronized as the noise is increased, but the pyramidal cells remain sharply synchronized. At the highest level of noise, the number of missed gamma cycles during the beta rhythm becomes irregular, but a clear underlying gamma rhythm remains. This behavior is also present in the experimental results described in the following section.

**3.1.6. In Vitro Experiments Corroborates the Predicted Temporal Separation.** Our simulation results showed that during the gamma rhythm,  $E_P$ -cells spike on every cycle, while  $E_S$ -cells are completely suppressed. During the beta rhythm, the  $E_S$ -cells fired, but on cycles different from those of the  $E_P$ -cells. To test these modeling predictions, we used five hippocampal slice preparations with drive to two neighboring sites of CA1. The sites are close enough to one another that the pyramidal cells share interneurons, a critical feature of the model network. One of the two sites was treated with potassium-free ACSF to transiently lower the excitability, mimicking the structured (sigmoidal) input to the model network, in which neurons were given high or low excitatory inputs. The goal of the experiment was to determine whether the combined network (both sites, including shared interneurons) responded to the differences in excitability by creating temporally separated cell assemblies, as in the simulations.

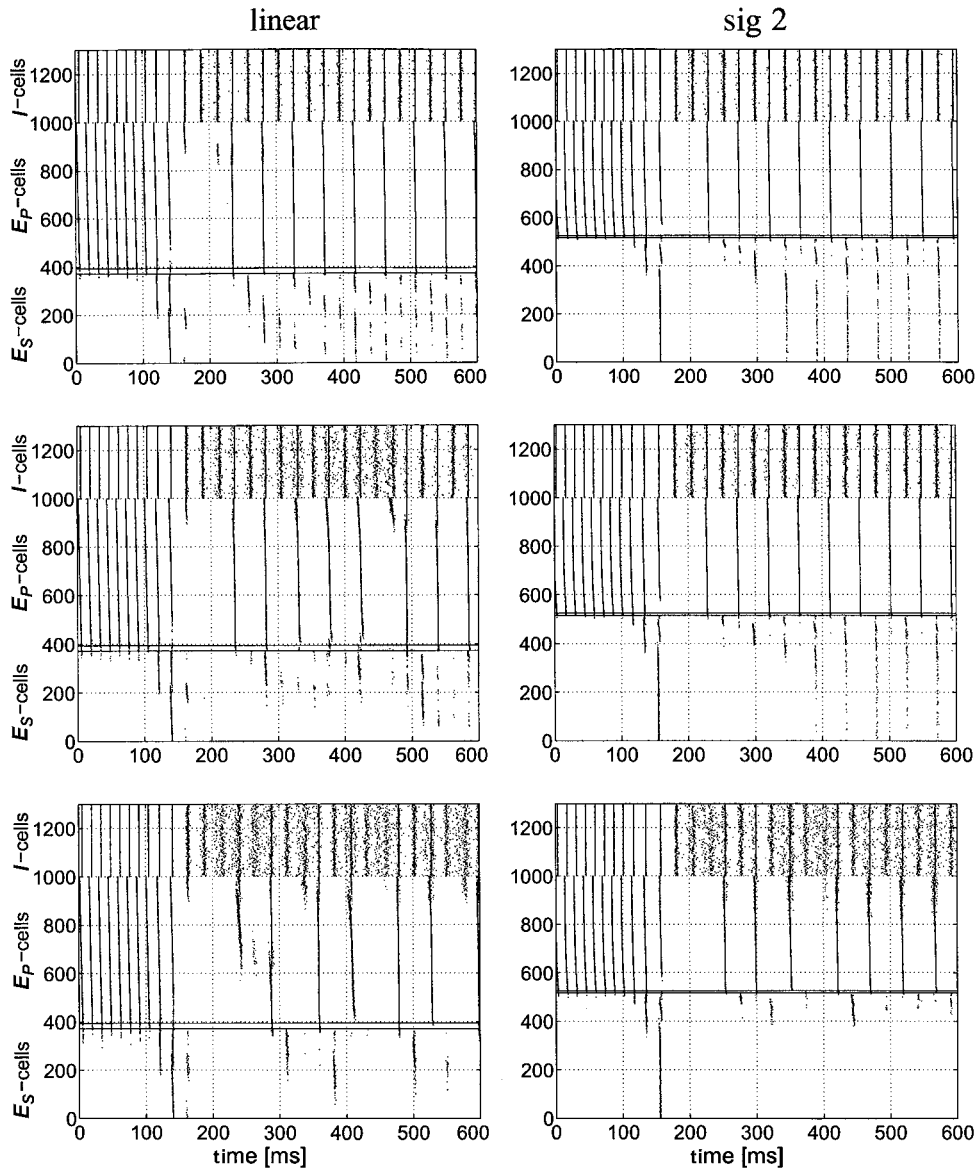
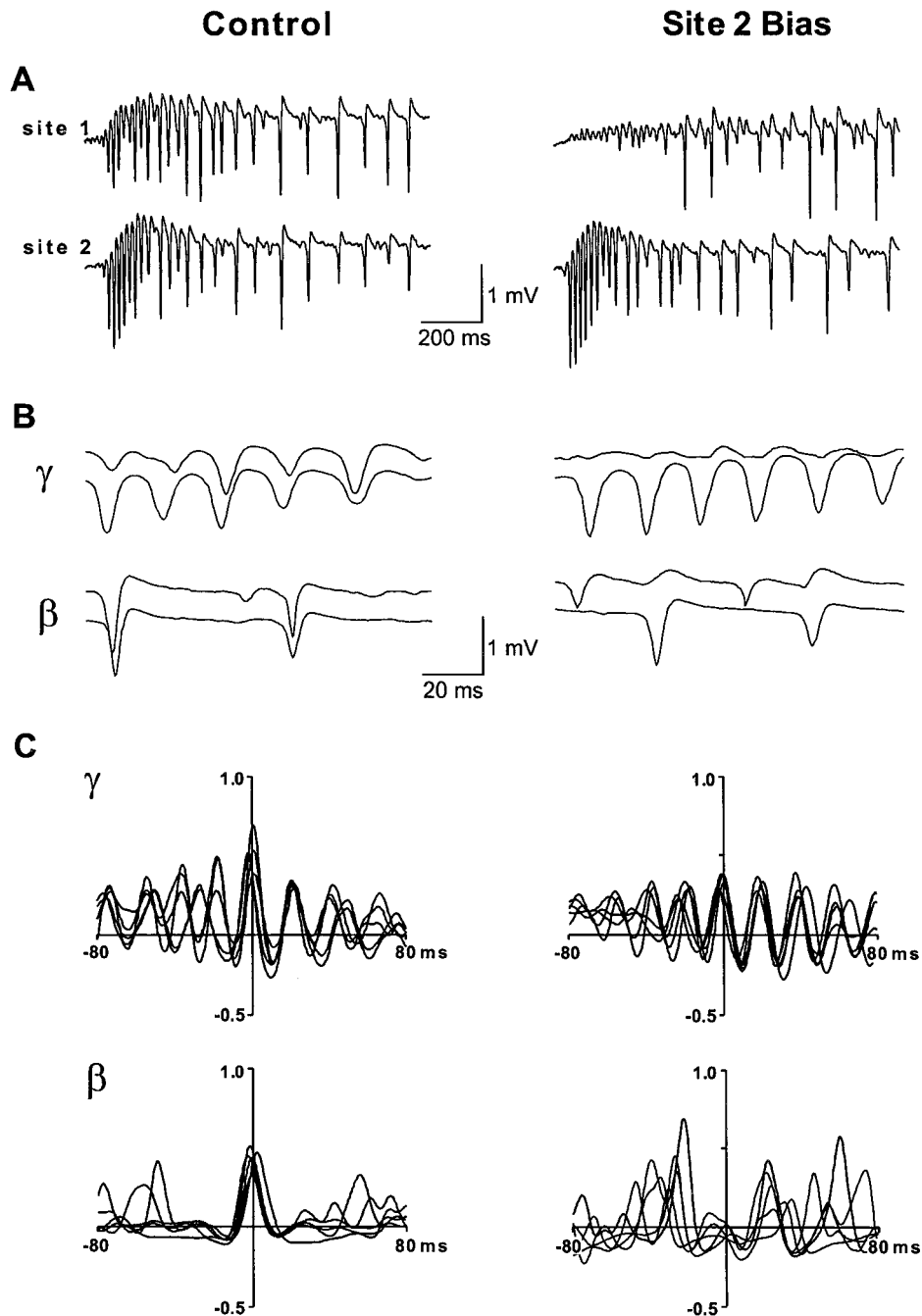


Figure 9. Effects of introducing noise in the applied currents to both  $E$ - and  $I$ -cells. The left column shows simulations with uniformly (i.e. linear) increasing drives, and the right column shows simulations with sigmoidally increasing drives (sig 2). The top graphs display results with a low level of noise ( $\sigma = 2 \mu\text{A}/\text{cm}^2$ ), the middle graphs displays results with an intermediate level of noise ( $\sigma = 4 \mu\text{A}/\text{cm}^2$ ), and the bottom graphs displays results with a high level of noise ( $\sigma = 6 \mu\text{A}/\text{cm}^2$ ).

Control conditions, with equal drive to both sites, produce a posttetanic response of a gamma rhythm followed by a beta rhythm. This is consistent with previous work using two more separated sites (Whittington et al., 1997). As shown in Fig. 10 (left panels), the firing times are synchronous (zero phase lag) between the two sites for both rhythms, again as expected from previous work (Whittington et al., 1997). Results for one slice

are shown in Figs. 10A and B; results from the remaining four slices were similar. Cross-correlation results for all five slices are shown superimposed in Fig. 10C.

A site bias is introduced by pressure ejection of potassium-free ACSF to one site. A 2 to 4 ms period of ejection produces a  $4.2 \pm 0.8$  mV hyperpolarization of pyramidal cell membrane potential at rest. This hyperpolarization lasted 200 to 400 ms and was thus



*Figure 10.* Temporal separation of beta oscillations by regional excitability bias in hippocampal area CA1. A shows concurrently recorded field potential oscillations at two sites separated by 0.8 mm starting immediately after the tetanic stimulations. Control recordings show both gamma and beta oscillations. Recordings in the site 2 bias condition show a large reduction in field potential amplitude during gamma activity and a smaller reduction during the later beta phase. Scale bars 1 mV, 200 ms. B shows expanded portions of the temporal relationship between gamma and beta oscillations at the two sites. The top trace of each pair is from site 1, and the bottom trace is from site 2. Scale bars 1 mV, 20 ms. C shows superimposed cross-correlograms between sites 1 and 2 from 5 gamma and beta oscillations in slices in control (left column) and site 2 bias (right column) conditions. Note the continued presence of synchrony at gamma frequencies in the site 2 bias condition but the presence of a phase lag equivalent to one or two gamma periods during the beta phase.

absent during the last part of the beta phase. When the pressure pulse is administered at the end of the tetanic stimulation, the number of action potentials observed in the pyramidal cells during the initial gamma rhythm is markedly reduced. This is reflected in the amplitude of the population spike component of field potential recordings (Fig. 10A). The field potential amplitude during the first 100 ms of oscillations is  $1.5 \pm 0.4$  mV in control (unbiased sites) and  $0.2 \pm 0.1$  mV following pressure ejection of potassium-free ACSF.

In the site bias case, as in the control case, the gamma rhythms are synchronous at the two sites, though very different in amplitude (see Fig. 10B, right panel). As predicted by the model, the subsequent beta rhythms are not synchronous; the field potentials show that the majority of the pyramidal cells in the site with lower excitability fire on different underlying gamma cycles than pyramidal cells in the other site. With on site bias, beta oscillations were highly synchronous between the two adjacent sites (for the five samples, the modular phase difference was  $2 \pm 1$  ms). However, with single site biasing, the modular phase difference was  $27 \pm 4$  ms for the five samples—approximately one gamma period.

We note that in Fig. 10A, the number of skipped gamma cycles per beta cycle is irregular. Thus, the experimental results resemble most clearly the simulation with the highest level of noise (see Fig. 9).

The clean temporal separation found in the model assumes that heterogeneity of the applied currents to the pyramidal cells remains unchanged during both the gamma and the beta rhythms. The separation between the two sites found in the experiment actually occurs under a weaker condition; the amount of heterogeneity in the pyramidal cell drives gradually wears off in the experiment during the beta rhythm. We have not yet found an experimental paradigm, with the two sites close enough to share common interneuronal systems, in which the applied currents remain different during both the gamma and the beta rhythms, as they may in an *in vivo* situation.

### 3.2. How Does Formation of Cell Assemblies Work?

In the following sections, we first explain how the cell assemblies are formed during the gamma rhythm and why changes of parameters are able to modulate the boundary between  $E_P$ - and  $E_S$ -cells. We then explain why cell assemblies do not form in networks displaying a beta rhythm in the absence of synaptic plasticity

during the gamma rhythm. Finally, we explain the most mysterious phenomenon: why synaptic modification during gamma facilitates the separation in time between cells participating in the gamma rhythm and cells suppressed during the gamma rhythm.

#### 3.2.1. The Gamma Rhythm

*Thresholds.* The existence of the threshold for participation in the cell assembly can be explained from the biophysical properties of the pyramidal cells and the control of the network by the interneurons. When interneurons fire, they inhibit pyramidal cells and also receive inhibition themselves. An interneuron is ready to fire again when the inhibition has worn off sufficiently to be counteracted by its tonic excitatory drive. Between one spike of the interneuron and the next, some of the pyramidal cells (those with enough drive) are able to fire before the next bout of inhibition; these are the pyramidal cells that fire in each succeeding cycle. There are no slow currents to provide memory that lasts much beyond one cycle; hence, the pyramidal cells that are subthreshold in one cycle remain subthreshold in the succeeding ones. The threshold is fairly sharp; only very few pyramidal cells are partially suppressed. The reason why these partially suppressed cells exist is that the pyramidal cells have a short memory arising from the fast-decaying delayed rectifier current. Because of this fast hyperpolarization, the cells that do not fire in a given cycle have a small comparative advantage over those cells that do fire. The cells whose drive places them near (but not over) their firing threshold are able to spike in the next cycle.

*Modulation of Thresholds.* Figure 11 illustrates how increasing mean drive to the *interneurons* changes the boundary between  $E_P$ - and  $E_S$ -cells. The figure shows that increasing the drive to the *I*-cells slightly decreases the time between two consecutive firings of an interneuron. This happens because the increase in *I*-cell drive make them recover faster from inhibition and thus enables them to fire earlier. The figure also shows that the interval from firing of the interneuron to firing of the  $E_P$ -cells with the strongest drive remains almost constant. This happens because the pyramidal cells recover from inhibition at the same rate, whatever the drive to the *I*-cells. As a result of these two effects, the interval from firing of the  $E_P$ -cell with the strongest drive to the next firing of the interneuron is reduced, and it is during this interval that the pyramidal cells with a weaker

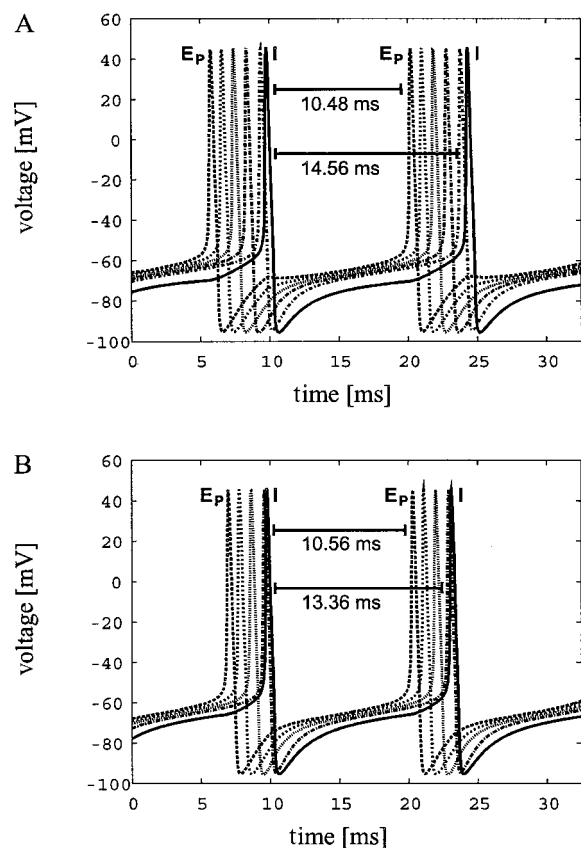


**Figure 11.** Effect on spike timing of increased drive to the *I*-Cells. The drive is increased by 100% (from  $1.0 \mu\text{A}/\text{cm}^2$  (A) to  $2.0 \mu\text{A}/\text{cm}^2$  (B)). The latency between firing of the first pyramidal cell and the previous interneuron spike remains almost constant (approximately 10.5 ms), but the interval between firing of two interneurons is decreased by 1.2 ms (from 14.56 ms (A) to 13.36 ms (B)). For technical reasons, this figure is generated using the small network, but a similar figure could be created using the large network.

drive fire. Hence, fewer pyramidal cells are able to fire before being silenced by the next bout of inhibition (the number of suppressed cells increases). In addition to changing the drive to the interneurons, their input can also be modulated by changing the strength of the *E*–*I* or *I*–*I* coupling. The effect of these manipulations are summarized in Table 2. The table represents change in one parameter while keeping the others at a base level. There are many other changes that could be made to show the robustness of our results, but because of the large number of parameters we are not able to include all of these in the current article. Changing the parameters beyond the changes shown in the table gives rise to new regimes where either the *E*-cells or the *I*-cells start to fire doublets. These parameter regimes are

beyond the scope of this article. Analogous explanations can be given in the case of decreased *I*–*I* coupling or increased *E*–*I* coupling.

Figure 12 illustrates how increasing mean drive to the *pyramidal cells* changes the boundary between *E<sub>P</sub>*- and *E<sub>S</sub>*-cells. In this example, the change in the number of suppressed cells occurs for a different reason than in the previous case, where the drive to the *interneurons* was increased; it is the effect of increased mean drive on the separation between *E*-cell spikes, rather than the change in timing between two consecutive firings of a given interneuron or pyramidal cell, that is responsible for the decrease in the number of suppressed cells. Note that, with the higher drive, more *E*-cells fire in a fixed interval than at the lower frequency, so more are able to fire before being suppressed by the response to the

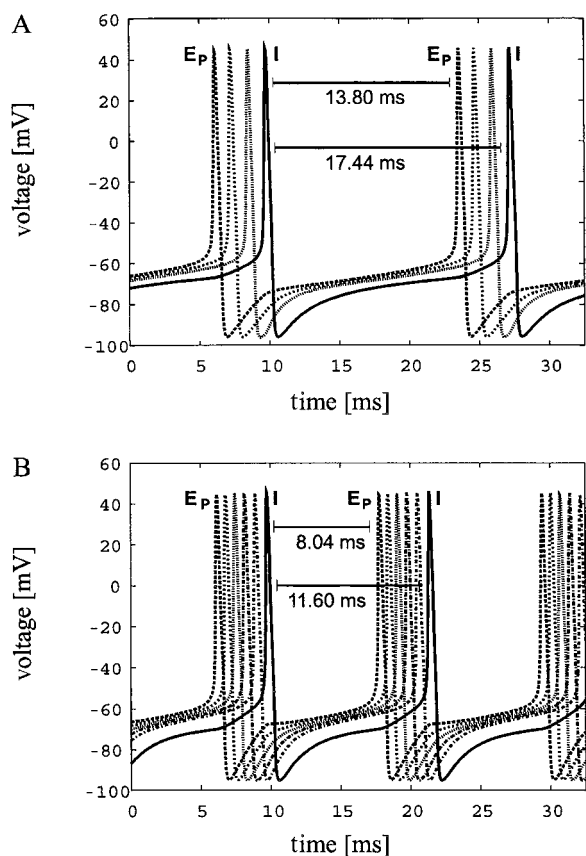


**Figure 12.** Effect on spike timing of increased mean drive to the *E*-cells. The mean drive is increased by almost 100% (from  $4.25 \mu\text{A}/\text{cm}^2$  (A) to  $8.125 \mu\text{A}/\text{cm}^2$  (B)), while the relative variation around the mean is kept constant. In this case, fewer cells are suppressed. Like Fig. 11, this figure shows results generated by the small network.

first  $E$ -cell spike. As in the previous paragraph, such changes can also be obtained by changing the strength of the  $I$ - $E$  coupling (see Table 3).

### 3.2.2. The Beta Rhythm

*Absence of Thresholds.* During the gamma rhythm, there is a sharp threshold between  $E_P$ - and  $E_S$ -cells because there are essentially no memory effects beyond one cycle. When slowly decaying currents (e.g., the  $M$ -current) are present, as in the beta rhythm, there are such memory effects. Thus cells that are suppressed during a given cycle may fire in a later cycle, when the slow outward current has diminished. As a result, there is no clean separation of the  $E$ -cell population into cell assemblies.

*Origin of Temporal Separation After Plastic Changes in Synapses.* To explain the temporal separation that occurs during the beta rhythm, two issues must be understood: why  $E_P$ -cells all fire at the same cycles and why  $E_S$ -cells fire out of phase with the  $E_P$ -cells. For clarity in this heuristic discussion, we refer to an “on-beat” cycle as one that ends with firing of  $E_P$ -cells and an “off-beat” cycle as one that ends with firing of  $E_S$ -cells (see Fig. 13).

It is easiest to understand the mechanisms involved in the separation in the case of zero coupling from the suppressed  $E$ -cells to the  $I$ -cells. In this case, when the beta rhythm is established, the underlying interneuronal gamma rhythm is not symmetric. That is, the off-beat cycle is always longer than the on-beat cycle (see Fig. 13A). This can be explained because firing of  $E_P$ -cells advance the firing of the following interneuron, while firing of  $E_S$ -cells do not advance (there are no  $E_S$ - $I$  connections) the firing of the  $I$ -cells (see Fig. 13A).

Now consider a cycle in which the  $E_P$ -cells fire at  $C_0$  (see Fig. 13A). The  $E_P$ -cells display an  $M$ -current, which slows their recovery and prevents them from firing in the next cycle (at  $C_1$ ). The  $E_S$ -cells, which do not fire at  $C_0$  and do not display an  $M$ -current, may be ready to fire in this cycle (at  $C_1$ ), and some do. The mysterious question is why, in the following cycle (at  $C_2$ ), when both  $E_P$ - and some  $E_S$ -cells have recovered from inhibition, only the  $E_P$ -cells fire. The answer to this question lies in the  $M$ -current and the differences in drive that defined the  $E_P$ - and  $E_S$ -cells. By the cycle ending at  $C_2$ , the  $M$ -current originating from the  $E_P$ -cells firing at  $C_0$  is now almost decayed. The  $E_S$ -cells

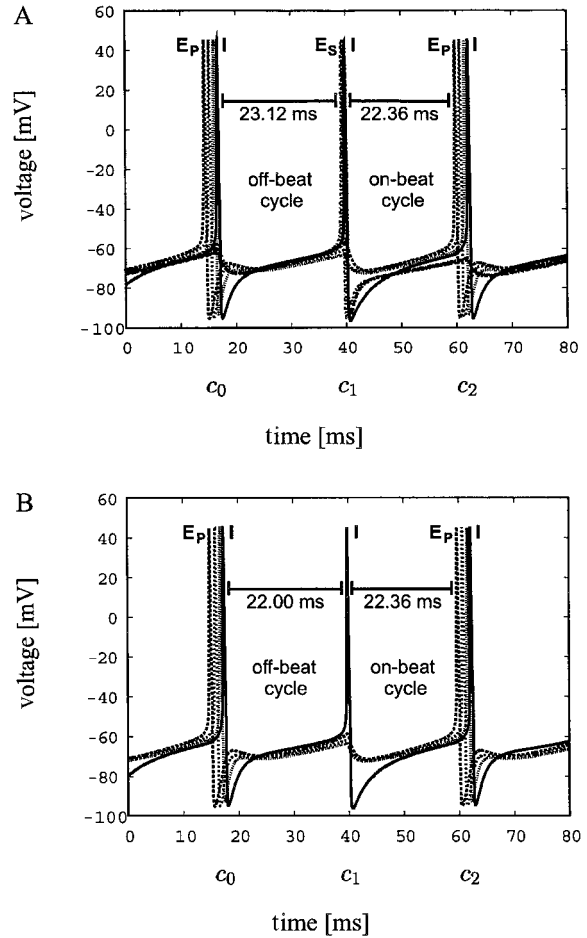


Figure 13. Subtle differences in timing between the off-beat intervals and the on-beat intervals. Without  $E_S$ - $I$  connections the  $I$ - $I$  interval is 23.12 ms (first interval in A), and with  $E_S$ - $I$  connections the  $I$ - $I$  interval for the off-beat interval is 22 ms (first interval in B); hence removing the  $E_S$ - $I$  connections expands the  $I$ - $I$  interval by 1.12 ms. However, the duration of the on-beat interval remains constant 22.36 ms (right column). Like Figs. 11 and 12, this figure shows results generated by the small network.

that fired at  $C_1$  are still inhibited by their  $M$ -current at  $C_2$ , but the  $E_S$ -cells that did not fire at  $C_1$  may be ready to fire. However, the  $E$ -cells that fire first in  $C_2$  ( $E_P$ -cells, by definition) are more excitable and hence are ready to fire earlier. Once they fire, the resulting inhibition “steps on” the  $E_S$ -cells and prevents them from firing in that cycle. As noted above, the off-beat cycles (e.g., the cycle ending at  $C_1$ ) are longer than the on-beat cycles (e.g., the cycle ending at  $C_2$ ), so  $E_S$ -cells can fire in those cycles without being suppressed by inhibition before they reach threshold. Finally, the  $E_P$ -cells are pulled into the same cycle by the  $E$ - $E$  coupling among them.

Note that if there is significant coupling from  $E_S$ - $I$ , there may not be a difference in the size of the on-beat and off-beat cycles or they may be reversed in size (see Fig. 13B). As a result the temporal separation can be degraded or eliminated. This is the reason that the decrease in the  $E_S$ - $I$  coupling is helpful in creating the separation. However, this regime does not require a complete absence of  $E_S$ - $I$  coupling (as in the above explanation); only that the coupling be sufficiently weak. The further the  $E_S$ - $I$  is decreased, the longer the difference between the off- and the on-beat cycles.

The difference in timing between off-beat and on-beat cycles is what enables the sigmoidal drives to create sharper temporal separations. As shown in Table 4, the sharper sigmoids have a larger difference between on-beat and off-beat cycles. The data in Table 4 also explains why it is not necessary to reduce  $E_S$ - $I$  when the sigmoid is sharp. For sig 2 and 3, the differences between on-beat and off-beat cycles remain large even when  $E_S$ - $I$  is not reduced. The table also shows that decreasing the drive to the  $I$ -cells sharpens the tempo-

*Table 4.* The table shows the length of the on-beat and the off-beat cycles as well as the difference between the two cycles for the drives used in Figs. 6 to 8. Drives marked with a \* correspond to simulations where  $E_S$ - $I$  has not been reduced. The table shows that for the sharper sigmoids and higher mean drives, the length of the off-beat cycle is significantly longer than the length of the on-beat cycles. This result corresponds to a more perfect temporal separation as shown in Figs. 6 to 7. The exception is the increased drive to the  $I$ -cells, where the on-beat cycle is longer than the off-beat cycle.

Modulation of synaptic drive to $E$ -cells			
Drive	On-beat cycle [ms]	Off-beat cycle [ms]	Diff [ms]
lin	22.36	23.12	0.76
lin*	22.00	22.36	0.36
sig 1	22.36	23.17	0.81
sig 1*	22.33	22.89	0.56
sig 2	22.05	23.39	1.34
sig 2*	22.01	23.20	1.19
sig 3	21.80	23.52	1.72
sig 3*	21.75	23.34	1.59
Mean 5.574	22.46	23.61	1.15
Mean 5.887	22.26	23.47	1.21
Mean 6.215	22.09	23.30	1.21
$I = 1.15$	23.79	25.59	1.80
$I = 1.3$	22.26	23.47	1.21
$I = 1.45$	22.16	21.28	-0.16

ral separation; the decrease from  $I = 1.3 \mu\text{A}/\text{cm}^2$  to  $I = 1.15 \mu\text{A}/\text{cm}^2$  results in a difference of almost 2 ms between on-beat cycles and off-beat cycle. The separation remains sharp even though some of the  $E_P$ -cells with high drives fire on every cycle of the underlying interneuronal rhythm. However, a similar increase in drive to the  $I$ -cells results in an almost total suppression of the  $E_S$ -cells both during the gamma and the beta rhythms, and the  $E_S$ -cells that do fire do so during the on-beat cycle. This can be also be explained from the “negative” difference between off-beat and on-beat cycles (the on-beat cycles are longer than the off-beat cycles). The short off-beat cycles make it almost impossible for the  $E_S$ -cells to recover from inhibition, and as a result they do not fire in these cycles. During the on-beat cycles, the firing of the  $I$ -cells is mainly controlled by the stronger driven  $E_P$ -cells, and hence only very few of the  $E_S$ -cells are able to fire. As a result, most of the  $E_S$ -cells remain suppressed both during the gamma and the beta rhythms.

In general, we can conclude that the temporal separation can be found for a wide choice of parameters, that introducing sigmoidally distributed drives to the pyramidal cells sharpens the temporal separation, and that if the sigmoid is sufficiently sharp, it is no longer necessary to reduce the  $E_S$ - $I$  coupling. The parameter change that affected our results the most was the drive to the interneurons. If the drive to the  $I$ -cells is too high, the  $E_S$ -cells remain suppressed both during gamma and beta, and if it is too low, the highest drive  $E_P$ -cells start to fire on every cycle. We note, however, that in these cases there are still well-defined cell-assemblies.

## 4. Discussion

### 4.1. Modeling

We have shown that a network displaying a gamma rhythm can create a sharp partition between cells with stronger versus weaker levels of drive; the former spike on every cycle, while the latter remain subthreshold. This threshold between participating and suppressed cells is affected by the average drive to the  $E$ - and  $I$ -cells and hence also by synaptic conductances. It is in this sense that a network displaying a gamma rhythm can “tune” a population, picking out a larger or smaller subset of cells to fire. Attentional mechanisms that change the average drive could thereby change the fraction of cells that participate in a cell assembly. When

the network is provided with ionic currents and recurrent excitation appropriate to the beta rhythm, there are no longer any completely suppressed pyramidal cells. There is also no temporal separation between the cells with stronger drive and those with weaker drive.

Synaptic changes associated with Hebbian plasticity alter the network, allowing a temporal separation between  $E_P$ - and  $E_S$ -cells during the beta rhythm. In a Hebbian manner, the recurrent excitation is strengthened among those pyramidal cells that participate in the gamma rhythm, and the excitation to the interneurons is weakened from those pyramidal cells that were suppressed in the gamma rhythm. The result is that the cells suppressed in the gamma rhythm are actively encouraged by the network dynamics to fire in different cycles from those participating in the gamma rhythm. There is now direct evidence for the increase in  $E-E$  connections in CA1 slices (Traub et al., 1999b; Whittington et al., 1997). Evidence for decreasing  $E_S-I$  connections was obtained in a context in which the postsynaptic cells were hyperpolarized (Traub et al., 1999b) rather than the presynaptic ones as in our model. Our modeling predicts and explains the off-cycle firing of pyramidal cells with a weak drive. We give experimental evidence of this predicted temporal separation in hippocampal slices. Experimental data demonstrate that interregional phase shifts of one underlying gamma period can exist in a stable fashion for many periods of a principal cell population beta oscillation. However, further experimental work is needed to establish whether this temporal relationship is brought about by mechanisms described in this article.

A surprising effect revealed by our modeling is that the facilitation or disruption of the temporal separation between  $E_P$ - and  $E_S$ -cells during the beta rhythm depends on subtle changes in spike timing. A reduction in excitation from the cells suppressed during the gamma rhythm ( $E_S$ -cells) changes the timing of the intervals between interneuron spikes by under 1.5 ms; yet this is enough to make a major difference in the temporal separation. (See Ermentrout and Kopell, 1998, Jones et al., 2000, and Kopell et al., 2000, for other examples of large effects of small changes in timing.) One might expect noise to abolish an effect based on such tiny changes, but noise actually strengthens the separation significantly. The simulations discussed above show that the effect occurs in large networks but does not depend on having large numbers of cells. It remains to be investigated how sparse coupling and diversity among the interneurons might affect the temporal separation.

The modeling work in this article is related most closely to that of Andrea Bibbig and to a series of papers by DeLiang Wang and collaborators. The model by Bibbig (1999, 2000) uses potentiation of  $I-E$  synaptic conductances (instead of activating a slow outward M-current) and enhanced  $E-E$  connections (similar to our model) to obtain a gamma-to-beta transition. As in our article, some  $E-I$  connections are weakened to obtain pattern separation. In her simulations, different groups of neurons are activated during separate epochs of gamma (with or without beta); if these groups later on are stimulated simultaneously, they become active at different phases of an oscillation or oscillate at somewhat different frequencies, creating a separation.

D. L. Wang and colleagues (Liu and Wang, 1999; Terman and Wang, 1995; Wang and Terman, 1997) investigated the ability of a collection of cells to segment a visual scene. As in the current work, oscillators that fire produce inhibition that suppresses other cells. Also, as in our preprocessed beta rhythm, excitatory connections among cells involved in the same assembly are critical to network behavior. A major difference between the work reported in these papers and the current work is the level at which the oscillators are described. The models of Wang and collaborators deal with relaxation oscillators described abstractly, while we use conductance-based models for spiking cells. The more detailed description allows us to address questions of how the particular ionic currents help to determine the synchronization properties of the network.

Other related modeling literature dealing with stimulus dependent synchrony of oscillations and visual segmentation is Chawanya et al. (1993), Grannan et al. (2000), Gray et al. (1989), König and Schillen (1991), and Sompolinsky and Golomb (1991). A paper using oscillations for contour extraction is Yen and Finkel (1997). Related work on formation of distinct synchronously active assemblies occurring in the context of nested theta and gamma rhythms is reported in Jensen and Lisman (1996a, 1996b). See also Kopell and Le Masson (1994).

#### 4.2. Functional Implications

The ability of the beta rhythm to maintain a well-defined cell assembly is significant because of the contexts in which this rhythm is found. In neocortical EEG, beta activity appears to be associated with long-range coherence in response to sensory stimulation (Classen et al., 1998; Roelfsema et al., 1997; von Stein et al.,

1999). Other work suggests that the beta rhythm is associated with higher-level processing, which is expected to involve long-range coordination. For example, beta EEG activity has been found to accompany successful feature extraction (Pfurtscheller et al., 1994). Similarly, in some cognitive tasks, while gamma activity increases with increased task difficulty, beta activity declines as features become harder to identify (Gross and Gotman, 1999). There is also evidence that beta oscillations are associated with selective attention (Gomez et al., 1998) and that reduced beta activity is associated with poor feature extraction ability in ADHD patients (Lazzaro et al., 1998).

Earlier analysis (Kopell et al., 2000) has shown that the biophysical properties of the beta rhythm are well matched to the task of long-distance synchronization. The long decay time of the M-current allows synchronization even in the presence of long conduction delays. Bibbig (1999, 2000) uses Hebbian plasticity to obtain somewhat longer allowable conductance delays in the gamma rhythm, though they are smaller than those obtained in the beta study by Kopell et al. (2000). Other analysis (Jones et al., 2000) shows that the longer interval of allowed conduction delays is not due simply to the longer period of the beta rhythm, since the still slower alpha rhythm, based on different ionic currents, does not synchronize well over long distances. This work is all based on the findings by Traub et al. (1996b) that spike doublets in *I*-cells are related to the ability to synchronize over significant conductance delays.

Although the functional significance of gamma and beta rhythms remains controversial, there is a large body of work (reviewed by Tallon-Baudry and Bertrand, 1999) demonstrating that the strength of an induced neocortical gamma rhythm can be modulated by parameters associated with perceptual and cognitive tasks. Thus, it is important to determine what biophysical parameters can influence the size of a gamma-synchronized cell assembly and to understand at a mechanistic level how input and modulations during cognitive tasks can affect synchronization at gamma frequencies. Sustained oscillatory activity in gamma and beta bands has been seen in EEG studies in a delayed-match-to-sample task (Tallon-Baudry et al., 1998; Tallon-Baudry et al., 1999). The gamma and beta bands are also prominent in a study of local field potentials and single-unit activity in macaque parietal cortex during working memory (Pesaran and Andersen, pers. comm.). Hence, the ability of the gamma rhythm to

facilitate temporal segregation of cell assemblies during the beta rhythm is potentially relevant to mechanisms of working memory.

Care must be exercised in comparing data from hippocampus and neocortex and in relating *in vitro* and *in vivo* work. Nevertheless, there are significant and suggestive similarities between *in vitro* and *in vivo* findings. For example, beta oscillations in CA1 have been shown to arise from preceding synchronous gamma activity *in vitro* (Traub et al., 1999b; Whittington et al., 1997), as is also demonstrated here. Similarly, in neocortical EEG studies in clinical settings (Haenschel et al., 2000), sensory-induced oscillations include a period of gamma followed by beta; the latter displays strong coherence with ongoing underlying gamma activity as in the hippocampal slice data. Furthermore, slice studies show that beta, but not gamma, habituates to spatially separated stimulation (Doheny et al., 2000), and a similar habituation is seen in clinical studies (Haenschel et al., 2000).

It has been shown that preprocessing of sensory signals by gamma oscillations can occur in the temporal domain (Joliot et al., 1994; Gray et al., 1989; Müller et al., 1996). Different phases of a gamma oscillation can be used to code for features of a sensory input when they are perceived to be separate, and synchrony occurs only when different features are similar enough to be considered parts of a single object. The present simulations and experimental data demonstrate an additional kind of gamma preprocessing, based on different levels of excitatory drive to different subsets of neurons. Such preprocessing results in a temporal separation during subsequent beta frequency oscillations. The “thresholding” effect of gamma oscillations suggests that gamma can actively segment neuronal activity induced by the most salient components of a sensory stimulus from activity induced by less salient components. Preprocessing of sensory inputs for subsequent beta frequency oscillations may thus perform an abstraction, reducing the size of the synchronous cell assembly, so that only those cells coding for the most salient features of an object transmit their temporal information (synchrony) to the beta component of the response.

### Acknowledgments

We thank S. Epstein, B. Ermentrout, and R. D. Traub for penetrating comments and questions during our writing of this article and P. Pacheco for help with

the simulations involving the NEUROSYS package. N. Kopell received support from NSF grant DMS-9706694 and NIH grant MH47150, M. S. Olufsen received support from NSF G.I.G. DMS-9631755, and M. Whittington received support from the Wellcome Trust.

## References

- Bibbig A (1999) Gamma-beta transition, pattern separation and the plasticity of inhibitory and excitatory synapses (abstract). *Soc. Neurosci. Abs.* 25: 2257.
- Bibbig A (2000) Oscillations, synchronization, pattern separation and Hebbian plasticity in networks of excitatory and inhibitory cells (in German). Ph.D. Thesis, Department of Neural Information Processing and Department of Computational Science, University of Ulm, Germany.
- Buhl EH, Tamas G, Fisahn A (1998) Cholinergic activation and tonic excitation induce persistent gamma oscillations in mouse somatosensory cortex *in vitro*. *J. Physiol.* 513(Pt. 1): 117–126.
- Chawanya T, Aoyagi T, Nishikawa I, Okuda K, Kuramoto Y (1993) A model for feature linking via collective oscillations in the primary visual cortex. *Biol. Cybern.* 68: 483–490.
- Chow C, White JA, Ritt J, Kopell N (1998) Frequency control in synchronized networks of inhibitory neurons. *J. Comp. Neurosci.* 5: 407–420.
- Classen J, Gerloff C, Honda M, Hallett M (1998) Integrative visuomotor behavior is associated with interregionally coherent oscillations in the human brain. *J. Neurophysiol.* 79(3): 1567–1573.
- Crook SM, Ermentrout GB, Bower JM (1998) Spike frequency adaptation affects the synchronization properties of networks of cortical oscillations. *Neural Comput.* 10(4): 837–854.
- Crook SM, Ermentrout GB, Vanier MC, Bower JM (1997) The role of axonal delay in the synchronization of networks of coupled cortical oscillators. *J. Comp. Neurosci.* 4: 11–172.
- Doheny HC, Faulkner JH, Gruzelier T, Baldeweg T, Whittington MA (2000) Pathway specific habituation of induced gamma oscillations in the hippocampal slice. *Neuroreport* 11(12): 2629–2633.
- Ermentrout GB, Kopell N (1998) Fine structure of neural spiking and synchronization in the presence of conduction delays. *Proc. Natl. Acad. Sci.* 95: 1259–1264.
- Farmer SF (1998) Rhythmicity, synchronization, and binding in human and primate motor systems. *J. Physiol.* 509(Pt. 1): 3–14.
- Faulkner HJ, Traub RD, Whittington MA (1999) Anaesthetic/amnesic agents disrupt beta frequency oscillations associated with potentiation of excitatory synaptic potentials in the rat hippocampal slice. *Br. J. Pharmacol.* 128: 1813–1825.
- Fries P, Reynolds JH, Rorie AE, Desimone R (2001) Modulation of oscillatory neuronal synchronization by selective visual attention. *Science* 291(5508): 1560–1566.
- Fries P, Roelfsema PR, Engel AK, König P, Singer W (1997) Synchronization of oscillatory responses in visual cortex correlates with perception in interocular rivalry. *Proc. Natl. Acad. Sci.* 94(23): 12699–12704.
- Gomez CM, Vazquez M, Vaquero E, Lopez-Mendoza D, Cardoso MJ (1998) Frequency analysis of the EEG during spatial selective attention. *Int. J. Neurosci.* 95(1–2): 17–32.
- Grannan ER, Kleinfeld D, Somplinsky H (2000) Stimulus dependent synchronization of neuronal assemblies. *Neural Comput.* 5: 550–569.
- Gray CM (1999) The temporal correlation hypothesis of visual feature integration: Still alive and well. *Neuron* 24: 31–47.
- Gray CM, König P, Engel AK, Singer W (1989) Oscillatory responses in cat visual cortex exhibit intercolumnar synchronization which reflects global stimulus properties. *Nature* 338: 334–337.
- Gross DW, Gotman J (1999) Correlation of high-frequency oscillations with the sleep-wake cycle and cognitive activity in humans. *Neuroscience* 94(4): 1005–1018.
- Haenschel C, Baldeweg T, Croft R, Whittington MA, Gruzelier J (2000) Gamma and beta frequency cortical oscillation in response to novel auditory stimuli: A comparison of human electroencephalogram (EEG) data with *in vitro* models. *Proc. Natl. Acad. Sci.* 97(13): 7645–7650.
- Halliwel JV (1982) M-current in human neocortical neurones. *Neurosci. Lett.* 67(1): 1–6.
- Halliwel JV, Adams PR (1982) Voltageclamp analysis of muscarinic excitation in hippocampal neurones. *Brain Res.* 250: 71–92.
- Hodgkin AL, Huxley AF (1952) A quantitative description of membrane current and its application to conduction and excitation in nerve. *J. Physiol.* 117: 500–544.
- Jefferys JGR, Traub RD, Whittington MA (1996) Neuronal networks for induced “40 Hz” rhythms. *Trends Neurosci.* 19: 202–207.
- Jensen O, Lisman JE (1996a) Novel lists of 7+/-2 known items can be reliably stored in an oscillatory short-term memory network: Interaction with long-term memory. *Learn Mem.* 3(2–3): 257–263.
- Jensen O, Lisman JE (1996b) Theta/gamma networks with slow NMDA channels learn sequences and encode episodic memory: Role of NMDA channels in recall. *Learn Mem.* 3(2–3): 264–278.
- Joliot M, Ribary U, Llinas R (1994) Human oscillatory brain activity near 40 Hz coexists with cognitive temporal binding. *Proc. Natl. Acad. Sci.* 91: 11748–11751.
- Jones SR, Pinto DJ, Kaper TJ, Kopell N (2000) Alpha-frequency rhythms desynchronize over long cortical distances: A modeling study. *J. Comp. Neurosci.* 9: 271–291.
- Kienker P, Sejnowski J (1986) Separating figure from ground with a parallel network. *Perception* 15: 197–216.
- König P, Schillen TB (1991) Stimulus-dependent assembly formation of oscillatory responses: I. Synchronization. *Neural Comput.* 3: 155–166.
- Kopell N, Le Masson G (1994) Rhythmogenesis, amplitude modulation, and multiplexing in a cortical architecture properties. *Proc. Natl. Acad. Sci.* 91: 10586–10590.
- Kopell N, Ermentrout GB, Whittington MA, Traub RD (2000) Gamma rhythms and beta rhythms have different synchronization properties. *Proc. Natl. Acad. Sci.* 97: 1867–1872.
- Lazzaro I, Gordon E, Whitmont S, Plahn M, Li W, Clarke S, Dosen A, Meares R (1998) Quantified EEG activity in adolescent attention deficit hyperactivity disorder. *Clin. Electroencephalogr.* 29(1): 37–42.
- Li Z (1999) Visual segmentation by contextual influences via intracortical interactions in the primary visual cortex. *Comput. Neural. Syst.* 10: 187–212.
- Liu X, Wang D (1999) Perceptual Organization Based on Temporal Dynamics. In: Moser MC, Jordan MI, Petsche T, eds. *Advances in Neural Information Processing Systems 12*. MIT Press, Cambridge, MA.

- Müller MM, Bosch J, Elbert T, Kreiter A, Sosa MV, Sosa PV, Rockstroh B (1996) Visually induced gamma-band responses in human electroencephalographic activity: A link to animal studies. *Exp. Brain. Res.* 112(1): 96–102.
- Pacheco P, Camperi M, Uchino T (2000) Parallel Neurosys: A system for the simulation of very large networks of biologically accurate neurons on parallel computers. *Neurocomput.* 32–33: 1095–1102.
- Pfurtscheller G, Neuper C, Mohl W (1994) Event-related desynchronization (ERD) during visual processing. *Intl. J. Psychophysiol.* 16(2–3): 147–153.
- Roelfsema PR, Engel AK, König P, Singer W (1997) Visuomotor integration is associated with zero time-lag synchronization among cortical areas. *Nature* 385: 157–161.
- Schanze T, Eckhorn R (1997) Phase correlation among rhythms present at different frequencies: Spectral methods, application to microelectrode recordings from visual cortex and functional implications. *Intl. J. Psychophysiol.* 26(1–3): 171–189.
- Shadlen M, Movshon JA (1999) Synchrony unbound: A critical evaluation of the temporal binding hypothesis. *Neuron* 24: 67–77.
- Sompolinski H, Golomb D (1991) Cooperative dynamics in visual processing. *Phys. Rev. A* 43: 6990–7011.
- Tallon-Baudry C, Bertrand O (1999) Oscillatory gamma activity in humans and its role in object representation. *Trends Cog. Sci.* 3(4): 151–162.
- Tallon-Baudry C, Bertrand O, Peronnet F, Pernier J (1998) Induced  $\gamma$ -band activity during the delay of a visual short-term memory task in humans. *J. Neurosci.* 18(1): 4244–4254.
- Tallon-Baudry C, Kreiter A, Bertrand O (1999) Sustained and transient oscillatory responses in the gamma and beta bands in a visual short-term memory task in humans. *Vis. Neurosci.* 16(3): 449–459.
- Terman D, Wang DL (1995) Global competition and local cooperation in a network of neural oscillators. *Physica. D* 81: 148–176.
- Traub RD, Jefferys JGR, Whittington MA (1997) Simulation of gamma rhythms in networks of interneurons and pyramidal cells. *J. Comput. Neurosci.* 4: 141–150.
- Traub RD, Jefferys JGR, Whittington MA (1999a) *Fast Oscillations in Cortical Circuits*. MIT Press, Cambridge, MA.
- Traub RD, Whittington MA, Buhl EH, Jefferys JGR, Faulkner H (1999b) On the mechanism of the gamma-beta frequency shift in neuronal oscillations induced in rat hippocampal slices by tetanic stimulation. *J. Neurosci.* 19(3): 1088–1105.
- Traub RD, Whittington MA, Colling S, Buzsáki G, Jefferys JGR (1996a) Analysis of gamma rhythms in the rat hippocampus *in vitro* and *in vivo*. *J. Physiol.* 493: 471–484.
- Traub RD, Whittington MA, Stanford IM, Jefferys JGR (1996b) A mechanism for generation of long-range synchronous fast oscillations in the cortex. *Nature* 383: 621–625.
- von Stein A, Rappelsberger P, Sarnthein J, Petsche H (1999) Synchronization between temporal and parietal cortex during multimodal object processing in man. *Cereb. Cortex* 9: 137–150.
- Wang DL, Terman D (1997) Image segmentation based on oscillatory correlation. *Neural Comput.* 9: 1623–1626.
- Wang X-J, Buzsáki G (1996) Gamma oscillation by synaptic inhibition in an interneuronal network model. *J. Neurosci.* 16: 6402–6413.
- Whittington MA, Traub RD, Faulkner H, Stanford IM, Jefferys JGR (1997) Recurrent excitatory postsynaptic potentials induced by synchronized fast cortical oscillations. *Proc. Natl. Acad. Sci.* 94: 12198–12203.
- Whittington MA, Traub RD, Jefferys JGR (1995) Synchronized oscillations in interneuron networks driven by metabotropic glutamate receptor activation. *Nature* 373(6515): 612–615.
- Whittington MA, Traub RD, Kopell N, Ermentrout GB, Buhl EH (2000) Inhibition-based rhythms: Experimental and mathematical observations on network dynamic. *Int. J. Psychophysiol.* 38(3): 315–3336.
- Yen S-C, Finkel L (1997) Salient Contour Extraction by Temporal Binding in a Cortically based Network. In: Moser MC, Jordan MI, Petsche T, eds. *Advances in Neural Information Processing Systems* 9. MIT Press, Cambridge, MA.